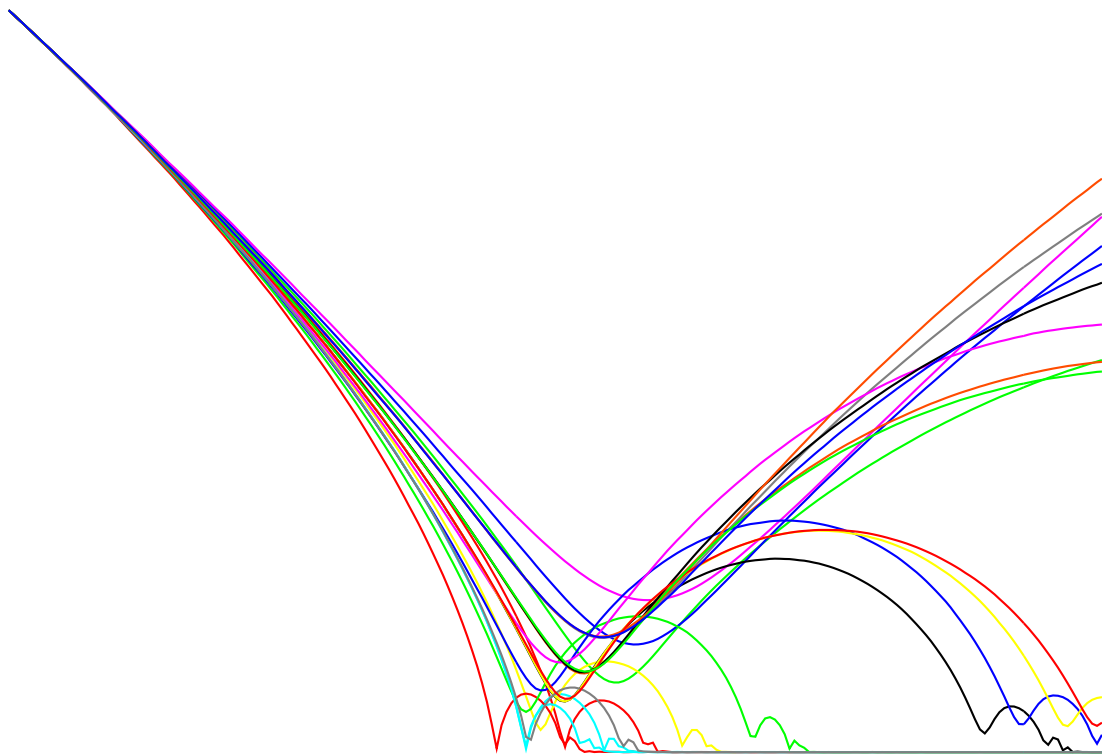


On the collision between the Milky Way and the Andromeda Galaxy

Master thesis, astronomy and astrophysics

J.C.J.G. Withagen

Supervisors: dr. S. Portegies Zwart and dr. S. Harfst



Sterrenkundig Instituut "Anton Pannekoek"
Universiteit van Amsterdam

Abstract

This paper argues, that using a recent estimated transverse velocity component of Andromeda of $v_{\text{trans}} = 42$ km/s, it will influence the time of merger between the two systems considerably. We present several models of the Local Group, using models which are derived from distribution functions of actual galaxies and evaluate them using N-body simulations. We performed our simulations using Graphic Processing Cards. We find that the two galaxies are not likely to collide in at least 9 Gyr and will not form the elliptical galaxy Milkomeda. We present evidence that this time of merger could be much longer than 9 Gyr, Most likely in the order of two Hubble times. We also performed a parameter study, varying v_{trans} , the total mass and the extent of Andromeda's halo, which resulted in constructing a parameter space we can use to test models with different total masses.

Subject heading: dark matter - galaxies: individual (M31) Galaxy: general - Local Group
- methods: N-body simulations

Preface

This thesis covers the work done during my masters project as part of the fulfillment of the Masters degree in astronomy and astrophysics at the University of Amsterdam. This research project was done under the supervision of dr. S Portegies Zwart and dr. S Harfst at the astronomical institute "Anton Pannekoek" from September 2007 until August 2008.

Table of contents

| | | |
|----------|--|-----------|
| 1 | Introduction | 1 |
| 1.1 | Galaxies | 1 |
| 1.2 | Galactic classification and evolution | 3 |
| 1.3 | The aim of this thesis | 7 |
| 1.4 | The outline of this thesis | 10 |
| 2 | Methods | 11 |
| 2.1 | The two body problem | 11 |
| 2.2 | Timing argument | 12 |
| 2.3 | N-body simulation | 13 |
| 2.4 | Galactics | 15 |
| 2.5 | Nemo | 16 |
| 2.6 | Simulations | 16 |
| 3 | Initial Conditions | 21 |
| 3.1 | Initial conditions of the Milky Way and Andromeda | 21 |
| 3.2 | Parameter study of the Milky Way Andromeda system | 22 |
| 3.3 | Initial conditions of the Milky Way Andromeda system | 23 |
| 4 | Results | 27 |
| 4.1 | Galactics | 27 |
| 4.2 | Separation versus Time | 39 |
| 4.3 | Formation of tidal tails | 44 |

TABLE OF CONTENTS

| | |
|--|-----------|
| 5 Discussion | 49 |
| 5.1 Mass produced by Galactics | 49 |
| 5.2 Mergers | 51 |
| 5.3 Size of Andromeda's halo | 55 |
| 5.4 Expanding bulge | 55 |
| 5.5 Conclusion | 56 |
| A Used derivations | 59 |
| B Tables and Figures | 65 |
| C Nederlandse samenvatting | 69 |
| D Used abbreviations | 71 |
| Bibliography | 73 |

CHAPTER 1

Introduction

Always majestic, usually spectacularly beautiful, galaxies are the fundamental building blocks of the Universe. The inquiring mind cannot help asking how they formed, how they function and what will become of them.

James Binney, 1987

1.1 Galaxies

Across the night sky is a band of light visible which we call the Galaxy or the Milky Way. The Greek name for the Milky way is derived from the word for milk, gala. In 1794 Charles Messier, published a catalog of 103 Nebulae. Object 31 in this cataloger is the Andromeda Galaxy. That is why this system is frequently named M31. Curtis (1917) detected in the “Great Andromeda Nebula” a few novae, which were much fainter compared to their counterparts in the Milky Way. This was the first clue that these observed spiral nebulae, like the Andromeda nebula, were perhaps extragalactic. In the debate that followed, Hubble (1929b) showed that these nebulae were in fact extragalactic objects, consisting of stars, dust and gas, using Cepheid variables to calculate the distance. When Zwicky (1933) and Smith (1936) discovered the evidence of dark matter it came clear that galaxies also have a huge component of dark matter.

Today the *Hubble Ultra Deep Field* shows us hundreds of galaxies are visible on a small part of the sky. This means that besides the Galaxy and Andromeda, there are literally hundreds of billions of other galaxies in the visible universe up to $z \approx 6$ (Beckwith *et al.*, 2006). The Local Group is our local system of galaxies in the Galactic Neighborhood. It consists of 46 objects. Of the Local Group member galaxies, the Milky Way and Andromeda galaxy are by far the most massive, and therefore the dominant members. Andromeda, see figure 1.1, is also known as Messier 31 (M31). Each of these two giant galaxies, has accumulated a system of satellite galaxies, which make up the other 44 members of the Local Group. The



Figure 1.1: This image shows the Andromeda galaxy. It is one of few distant objects which can be seen with the unaided eye. Also, two of its companion dwarf elliptical galaxies, M32 and M110 are visible in this picture. The galaxy above Andromeda is M32 and below Andromeda is M110. Photo Credits: Tony Hallas

most known satellites of the Milky Way are the Large and Small Magellanic Clouds. Both M31 as the Milky Way are spiral galaxies (Easton, 1913).

We can generally subdivide disk galaxies in a few parts:

- **Stellar disk.** The disk is the flat part of a galaxy. It is the most distinctive part of a galaxy, because of the spiral arms. The sun is situated in the disk, in one of the Milky Ways spiral arms. The star component of the galactic disk is called the stellar disk. The disk contains the most young stars in the galaxy.
- **Gaseous disk** The gas and dust components of the galactic disk are called the gaseous disk. It mostly consist of neutral hydrogen Wong *et al.* (2008).
- **Bulge.** The bulge is the spheroidal area where the central core of the galaxy is situated. In elliptical and spiral galaxies the nucleus corresponds with the area where the optical brightness reaches a maximum. In general bulges in the Local Group and its neighbors are reasonably old, with near-Solar mean abundance and can be seen as the more dissipated descendants of their halos (Wyse *et al.*, 1997)
- **Stellar halo.** This spherical region is filled with a few stars and globular clusters, which are dense collections of stars of typically one million stars.
- **Dark matter halo** The halo is the most massive part of a galaxy. It contains dark matter. The radius of this halo stretches much further then the radius of the disk. In some models these halo radii even overlap each other. The density structure, mass and size of the halo are still debated in the literature. Assumed is that the density decrease

according to the NFW profile (Navarro *et al.*, 1996). Although a consensus is not yet found.

- **Central black hole.** In the center of a galaxy is a super massive black hole situated, with mass in the order of 10^5 between $10^{11}M_{\odot}$. The mass the black hole in the center of the Milky Way, Sgr A*, is estimated to be $3.28 \pm 0.13 \cdot 10^9 M_{\odot}$ (Aschenbach, 2005).

All these parts are schematically represented in figure 1.2.

Morphology of the Milky Way

It was not until the mid-1950s that astronomers judged there was conclusive evidence of the Milky Way's spiral structure with its core in the direction of Sagittarius. Easton (1913) first sought photographic evidence that the Milky Way had in fact a spiral structure. This became more plausible when Hubble (1929a) found out that the spiral nebulae were extragalactic. Oort (1941)¹ suggested that hydrogen in interstellar space might emit an observable radio line. Reber (1944) plotted static radio noise in the sky not long after that. Seven years later the, now famous, 21 cm line was observed by Ewen and Purcell (1951) and Muller and Oort (1951) and they used it to unravel the Galaxies fine structure for the first time (Oort, 1953). This was possible because radio frequencies are almost unaffected by obscuring dust in the disk. A recent mapping of the Milky Way by Levine *et al.* (2006), see figure 1.3, shows a spiral structure. Figure 1.4 shows a artistic impression of the disk of our Galaxy and location of the sun.

Rotational Curve

All galaxies interact gravitationally with each other and rotate. The sun has an orbital period of ≈ 220 million years (Kerr and Lynden-Bell, 1986). The period of objects in a galaxy depends on the Radius from its center. A typical rotation curve is plotted in figure 1.5. These famous curves are direct evidence for the existence of dark matter in the Universe. The figure shows the rotation curve induced by the gravity potential of the disk. The observations show that, the disk alone cannot support the rotational velocities. They are higher and have a flat profile. Also plotted in this figure are the rotational velocities induced by the gravity potential of the dark matter halo. When you combine both potentials plot the induced rotational velocities it fits the observations. This is direct evidence for the existence of the dark matter halo and therefore evidence for the existence of dark matter in general.

1.2 Galactic classification and evolution

The galaxies we observe in the Universe at the present show a remarkable variety of properties. They vary in mass, size, morphology, color, luminosity and dynamics. Some galaxies are

¹Oort did this during the Nazi German occupation, while he was director of the Leiden Observatory. Despite the war, copies of the Astrophysical Journal still reached the Observatory in Leiden.

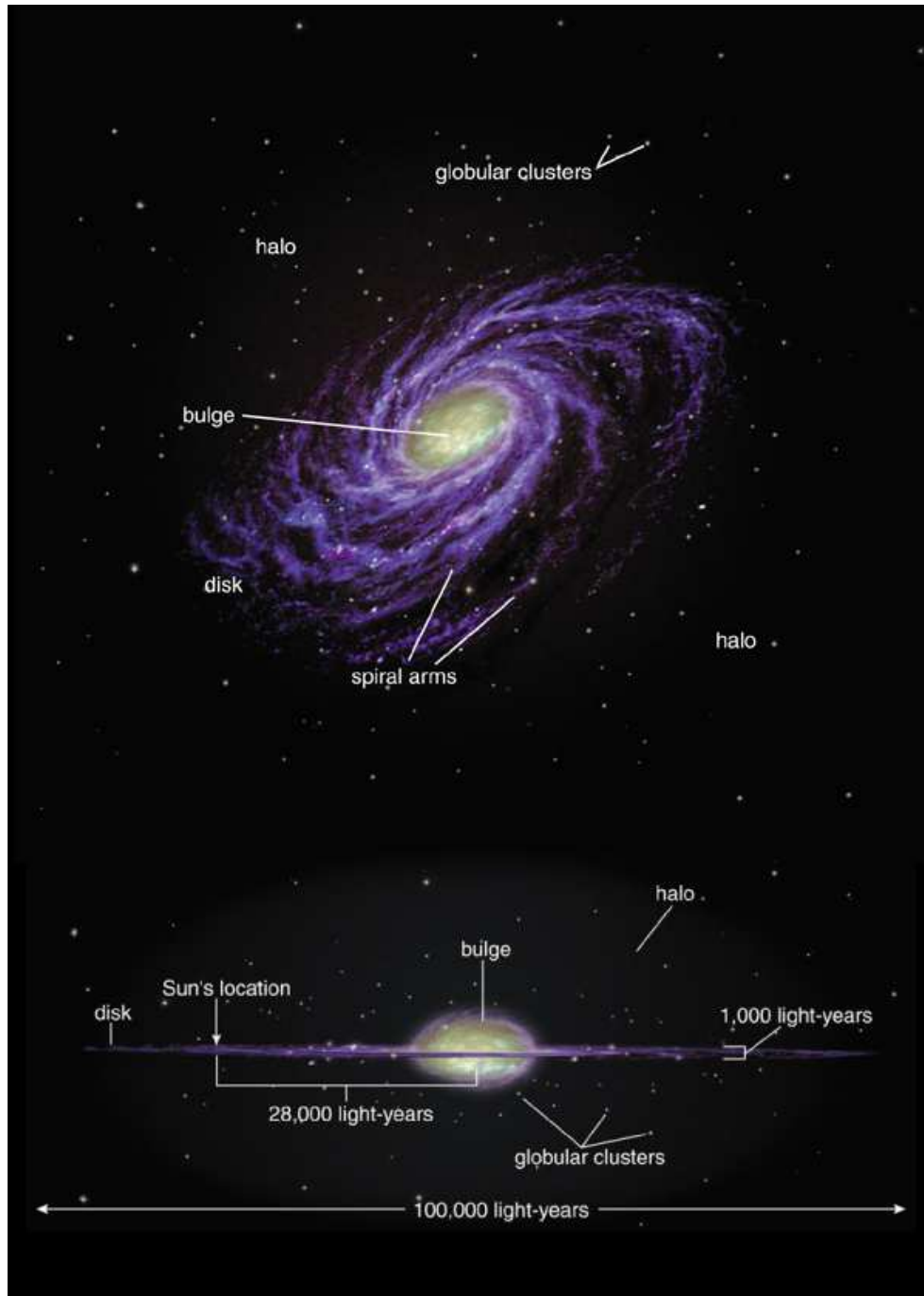


Figure 1.2: These are two artistic impressions of our Galaxy. The inner part is called the bulge. This bulge is located in the center. Our sun is located in the disk. The disk is surrounded by the most massive part of a galaxy, called the halo, which is filled with dark matter and globular clusters. These globular clusters are groups of old highly concentrated groups of stars in orbit of the galaxy. (Photo credit: Adison Wesley, Pearson Education, 2004)

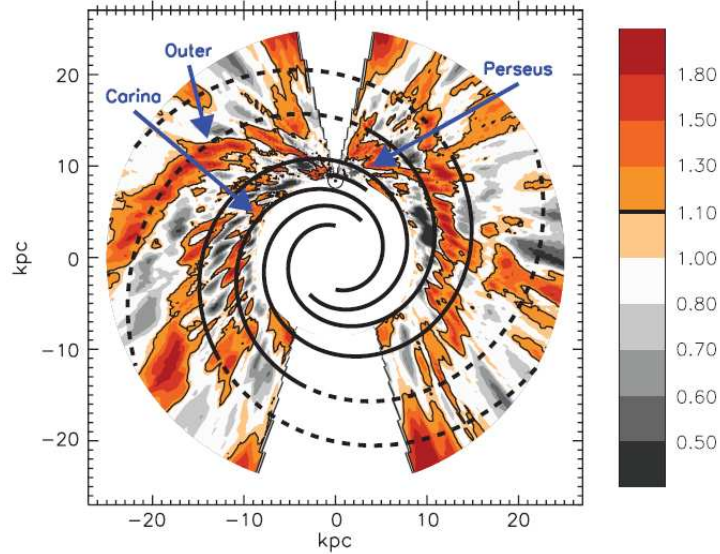


Figure 1.3: A detailed map of the surface density of neutral hydrogen in the Milky Way disk, demonstrating that the Galaxy is a non-axisymmetric multi-armed spiral galaxy. The colors correspondent with the detection of neutral hydrogen. (Photo credit: Levine *et al.* (2006))

hundreds of times brighter than our own Galaxy, while others can have one thousandth its luminosity. During the first half of the 20th century Hubble (1927) made a classification of galaxies based on their morphologies. Figure 1.6 shows the visualization of this Hubble classification scheme. He divided the galaxies in to four distinctive groups:

- Ellipticals
- Lenticulars
- Spirals
- Irregulars

Ellipticals are spheroid or elliptical galaxies with only a distinctive bulge and have no disk. Lenticular galaxies are elliptical with a very thin disk. Spiral galaxies have both disk and bulge. A spiral is barred when the spiral arms do not start at the center but at the extremities of a bar inside the bulge. Irregular galaxies are galaxies which cannot be classified by the other groups. Both Andromeda and Milky way are spiral galaxies. Andromeda is a Sb type and the Milky Way is believed to be a SBbc type galaxy. It was believed when this scheme was made, that all these classifications were galaxies in different stages of evolution. This idea is rendered obsolete (Strom and Strom, 1982).

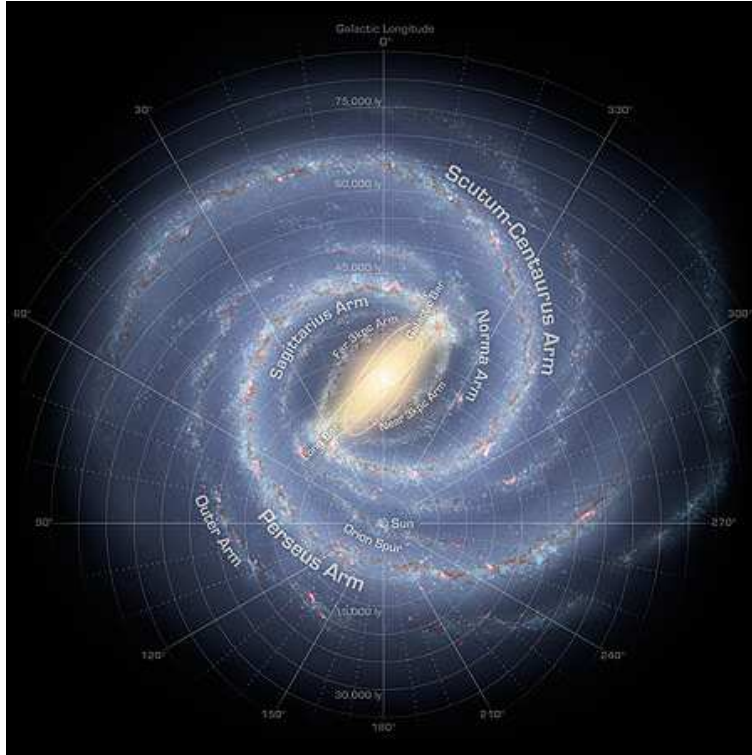


Figure 1.4: This image shows an artist impression of our current view of the Milky Way. The sun is located in the Orion Spur between the Scutum-Centaurus Arm and the Perseus Arm. (Photo credit: NASA/JPL-Caltech)

Mergers

An important mechanism that drives galaxy evolution is merging. Merging of galaxies is observed at all epochs where galaxies are detected. These events have major impact on morphology and promote an increase in star formation over a short period of time. The star formation increases when the gas and dust gets perturbed by a merger. The Jeans criteria can be exceeded locally by these perturbations, so that matter will collapse into stars. The final structure after merging may not have any resemblance of the original components. The outcome depends on their mass, rotation and type.

If two galaxies merge with similar mass, the gravitational perturbation throughout the galaxies moves very quickly. It takes place in short time of the order of the free-fall timescale,

$$t_{\text{ff}} = \frac{1}{2} \sqrt{\frac{R^3}{GM}} \quad (1.1)$$

Where R and M are the size and the mass of the galaxy. The free fall time, t_{ff} for our Galaxy is about 10^7 to 10^8 years. This process is called violent relaxation and produces a spheroid system. The emerging galaxy will look like a E0 galaxy (see figure 1.6). When two spiral galaxies merge, like in our case, their discs are destroyed. This results in a violent burst of

star formation. This can produce a galaxy with more stellar mass than both original galaxies combined.

When two galaxies merge with very different masses, the small galaxy will be destroyed and will be added to the large one. The gravitational perturbations are much smaller in this case and this enables the heavy galaxy to retain its properties and morphology. The Andromeda galaxy in fact has two nuclei (Lauer *et al.*, 1993). This could be the result of an earlier merger event, between M31 and a much less massive galaxy.

1.3 The aim of this thesis

The universe is expanding according to Hubble (1929a). You would expect that from a cosmological perspective the Milky Way and Andromeda move away from each other, but observations show us that the Milky Way and Andromeda are moving towards each other. But the influence of Hubble's law on the Local Group is insignificant compared with the relative velocities of its members. The expansion of the Universe starts becoming significant on larger scales, like 10 Mpc's. It is generally assumed that the Milky Way and Andromeda Galaxies move towards each other due to their mutual gravitational pull. Therefore we assume in our models classical Newtonian dynamics.

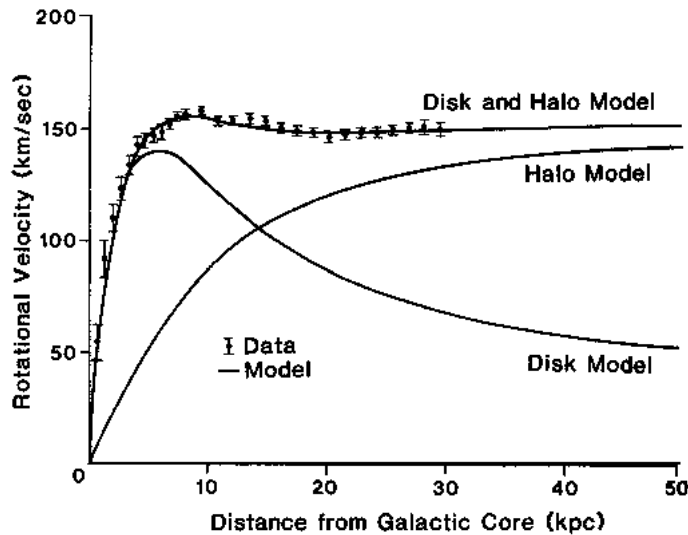


Figure 1.5: This plot shows the rotational curve of NGC 3198. The upper curve, with the data points, is a typical rotational curve of a spiral galaxy. The two other curves are expected contributions to this curve from the disk and the halo of the galaxy. This plot shows us that the disk cannot be the support these rotational velocities and is direct evidence for the existence of dark matter. (Photo credit: Binney and Tremaine (1987, chap. 10.1))

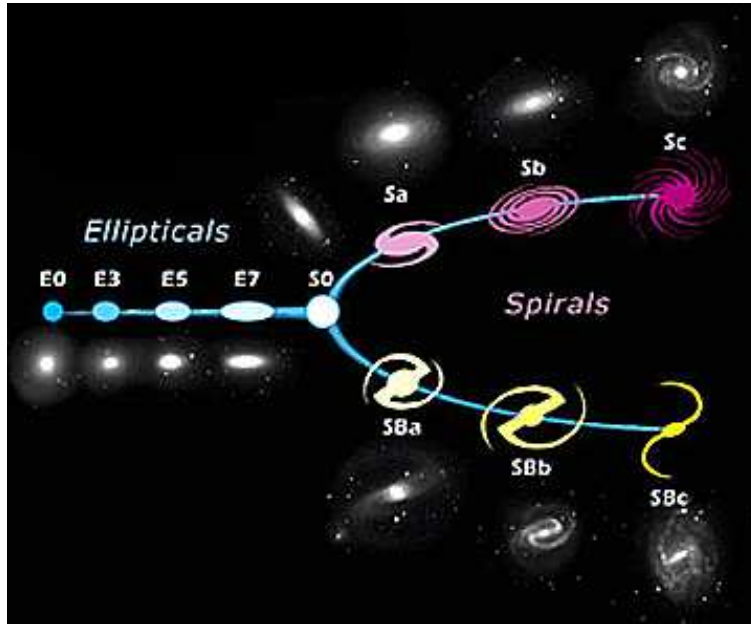


Figure 1.6: This figure shows the Hubble classification scheme. On the left are the elliptical galaxies and on the right the spirals. The spirals are divided in two groups, normal and barred spirals. Irregular galaxies are not shown in this graph. (Photo credit: STScI IPO)

It is relatively easy to measure the radial velocity of M31 accurately using Doppler shifts of known tracers, like supernovae or masers. This investigation began by Slipher (1913). It showed us that M31 is in fact moving towards us. The transverse velocity is much more difficult to measure. With our current equipment it is not directly observable, because of the long distance. Generally in models of the Milky Way Andromeda evolution the transverse velocity is set to zero. A recent article by van der Marel and Guhathakurta (2008) reports an indirect measurement of the transverse velocity by looking at the orbits of M31's satellites. The existence of a transverse velocity component of M31 can have a major effect on the fate of our Galaxy. It can enable Andromeda to miss the Milky way altogether in the future. In this thesis we evaluate the evolution of the Milky Way Andromeda system for different transverse velocities. We will also investigate the influence of the total mass and the radius of the galaxies halos on the system's evolution.

We perform a parameter study of the Milky Way Andromeda system to investigate under what conditions a merger between the two galaxies will take place. We will also look at the morphology of the systems during the collision and merged system. We expect the formation of tidal features like tidal tails, see figure 1.7. For the parameter study, we will vary three parameters:

- The magnitude of the transverse velocity component of the relative velocity of Andromeda, v_{trans} .

- The total mass of the Milky Way Andromeda system, M_{tot} .
- The size of the outer radius of the halo of Andromeda, $R_{\text{h,M31}}$.

In all these three circumstances we keep the mass ratio of both galaxies constant, so that

$$\frac{M_{\text{MW}}}{M_{\text{M31}}} \simeq \text{constant}. \quad (1.2)$$

$\mathbf{v}_{\text{trans}}$

First we will vary the V_{trans} keeping all other parameters fixed. We evaluate the system with various factors of the velocity given by van der Marel and Guhathakurta (2008). These factors are 0, 0.5, 0.8, 1, 1.2.

M_{tot}

Then we vary the total mass of the system. We can change the mass by changing the three halo parameters of the Galactics. This however results in models of Andromeda and the Milky Way which do not correspond anymore with observed rotational curves. We vary the total mass, M_{tot} , with factors of 0.7, 1 and 1.3 and evaluate the system for different $\mathbf{v}_{\text{trans}}$. Here we have kept the halo radius of both systems fixed.



Figure 1.7: This figure shows an object, in the southerly constellation Corvus, called the Antennae. It consists of two galaxies, NGC 4038 and NGC 4039. They are colliding and show far-flung arcing structures, known as tidal tails. (Photo credit: Daniel Verschate, Antilhue Observatory)

R_{halo}

We keep the total mass fixed and vary the radius of Andromeda's halo. This results in situations where the halo's of both systems do or do not overlap, when evaluating for different v_{trans} . We vary this radius by factor of 0.5, 1 and 1.5. In the last situation the halo's overlap, resulting in the increase of dynamical friction. On the other hand, using a small radius results in a situation where the radii will never overlap.

1.4 The outline of this thesis

Our thesis has the following outline:

In chapter 2 we show the methods we used in order to evaluate galactic dynamics of the Milky Way - Andromeda system. In this chapter we discuss basic N-body simulations. Starting from the 1-body problem, to the 2-body problem to the N-body problem.

Then in chapter 2.6 we will discuss how we evaluate our N-body problem. We will show what type of numerical methods and hardware we use.

The initial conditions for our N-body problem are defined and described in chapter 3. The properties of the individual galaxies greatly depend on the initial conditions. Also the properties of the total system are defined here.

In chapter 4 all our results are displayed. We show the stability of the galaxies we constructed and plot their separation versus time.

In the last chapter, 5 our conclusions are presented and we discuss them.

CHAPTER 2

Methods

In this chapter we will discuss the methods we use to work on the dynamics between the Milky Way and Andromeda Galaxy. The first part of this chapter is about analytical methods and the second part is about numerical methods.

2.1 The two body problem

Suppose we want to calculate how long it takes for two galaxies A and B to fall towards each other and hit under their own gravitational force. First of all we assume that both galaxies are point particles. Particle A has mass, M_A and particle B has mass, M_B . We suppose that M_A and M_B are the same. We define

$$M_{\text{total}} \equiv M_A + M_B. \quad (2.1)$$

Particle A and B are separated by distance R and have a initial radial velocity \mathbf{v}_0 . We call this problem the two body problem. We can solve this by using equation (2.2), Newtons second law (Newton, 1686). This problem was already solved by Kepler *et al.* (1609). We begin with Newton's second law,

$$\ddot{\mathbf{r}} = \frac{-GM_{\text{tot}}}{\mathbf{r}^2}. \quad (2.2)$$

Then we integrate the equation over time,

$$\int \ddot{\mathbf{r}} \dot{\mathbf{r}} dt = - \int \frac{GM_{\text{tot}}}{\mathbf{r}^2} \dot{\mathbf{r}} dt. \quad (2.3)$$

This results in the following equations,

$$\frac{\dot{\mathbf{r}}^2}{2} = \frac{GM_{\text{tot}}}{\mathbf{r}} + C, \quad (2.4)$$

$$|\mathbf{v}_0| = \sqrt{\frac{2GM_{\text{tot}}}{R} + 2C}. \quad (2.5)$$

We define \mathbf{v}_0 as the current relative velocity of both systems and R as current separation. For these boundary conditions we use the following integration constant,

$$C = \frac{\mathbf{v}_0^2}{2} - \frac{GM_{\text{tot}}}{R}. \quad (2.6)$$

Now we evaluate the system over time by integrating it again,

$$\frac{dr}{dt} = \sqrt{\frac{2GM_{\text{tot}}}{r} + \mathbf{v}_0^2 - \frac{2GM_{\text{tot}}}{R}}, \quad (2.7)$$

$$\frac{dt}{dr} = \sqrt{\frac{2GM_{\text{tot}}}{r} + \mathbf{v}_0^2 - \frac{2GM_{\text{tot}}}{R}}^{-1}, \quad (2.8)$$

$$\int_0^{t_{\text{end}}} dt = \int_R^0 \left(\frac{B}{r} + A \right)^{-\frac{1}{2}} dr. \quad (2.9)$$

Where

$$A = \mathbf{v}_0^2 - \frac{2GM_{\text{tot}}}{R} \quad (2.10)$$

and

$$B = 2GM_{\text{tot}}. \quad (2.11)$$

Using this method we can make an estimation when the Milky Way would hit Andromeda.

2.2 Timing argument

To get more insight in the orbit of the Milky Way and Andromeda we use a line of reasoning called the timing argument, first taught of by Kahn and Woltjer (1959). Let us assume again for the moment they are point masses and use the equation of motion from Newton (1686),

$$\frac{d^2r}{dt^2} = -\frac{GM_{\text{tot}}}{r^2}. \quad (2.12)$$

where M_{tot} is the total mass of the Milky Way and Andromeda combined and r is the distance between them. Now we assume that at $t = 0$, time of the big bang, the both (proto)galaxies were approximately at the same place, $r \approx 0$. Now assume that after $t = 0$ they start moving away from each other, due to Hubble expansion. This process is slowed by their gravitational pull. Let also assume that there is enough mass present what causes them to stop moving away from each other and fall back in a bound orbit. With these assumptions we can solve the differential equation (2.12) in parametric form (Kroeker and Carlberg, 1991). In a Keplerian potential the separation of the binary and time since pericenter are described by r and t .

$$r = a(1 - e \cos \theta) \quad (2.13)$$

$$t = \left(\frac{a^3}{8GM_{\text{tot}}} \right)^{\frac{1}{2}} (\theta - e \sin \theta) \quad (2.14)$$

Here a is the semi-major axis, e is the eccentricity and θ is the eccentric anomaly. The distance r ranges from 0 to R . $r = 0$ when $\theta = 0$ and $r = R$ when $\theta = \pi$. These results give the relative velocity v ,

$$v = \frac{dr}{dt} = \frac{dr}{d\theta} \frac{d\theta}{dt} = \left(\frac{2GM}{a} \right)^{\frac{1}{2}} \left(\frac{\sin\theta}{1 - \sin\theta} \right) \quad (2.15)$$

$$v = \frac{r \sin\theta(\theta - \sin\theta)}{t(1 - \cos\theta)^2} \quad (2.16)$$

assuming that the orbit is radial and therefore $e = 1$. When we put r and t to the left hand side we get

$$\frac{vt}{r} = \frac{\sin\theta(\theta - \sin\theta)}{(1 - \cos\theta)^2}. \quad (2.17)$$

This equation can be solved for θ because the left-hand side consists purely of observable quantities. We take for the time, t , the age of the universe, 13.7 Gyr (Spergel *et al.*, 2007) and for r the distance between the MW and M31, 770 kpc (McConnachie and Irwin, 2006), (Ribas, 2004). For v for the moment we only assume the well known radial velocity, 130 km s^{-1} , (Courteau and van den Bergh, 1999). Now we can calculate θ numerically. With this method we can find a value for the semi-major axis a and the total mass M_{tot} of the binary system. This method is used to obtain an upper limit for the mass of the local group and the age of the Universe.

2.3 N-body simulation

At large distances, we can assume that galaxies are point masses. However, we can no longer assume this, when the distance between the galaxies is too small. Then dynamical friction starts to play a role. Also information about the morphology of the galaxies is lost when you assume they are point masses. Therefore we need a method that describes a galaxy as a collection of individual gravitationally bound point particles instead of a single particle.

When calculating the dynamics for three or more particles you cannot use the above methods to find an analytical solution. Dynamical systems with three or more particles are chaotic in nature and was in the 18th century the basis for chaos theory. When we want to evaluate these two systems of gravitationally interacting particles we need to solve the following equation for every particle:

$$\mathbf{F}_i = \sum_j \frac{Gm^2(\mathbf{x}_j - \mathbf{x}_i)}{(|\mathbf{x}_i - \mathbf{x}_j|^2)^{\frac{3}{2}}}. \quad (2.18)$$

Equation (2.18) is the basis of N-body simulation. We can calculate the force acting on every particle from every particle and solve the equations of motion for every particle per discrete time step. Integrating over these discrete time steps gives us the dynamics of the system. This numerical technique has given us most of our current understanding of Galactic dynamics, according to Binney and Tremaine (1987, chap 2.8).

Softening

Equation (2.18) has, however, a singularity in it when two particles collide. This makes the denominator approach zero. To prevent this singularity we can add an extra parameter to equation (2.18). We will add a minimal value, ϵ for the separation between individual particles. Equation (2.18) is rewritten to

$$\mathbf{F}_i = \sum_j \frac{Gm^2(\mathbf{x}_j - \mathbf{x}_i)}{(\epsilon^2 + |\mathbf{x}_i - \mathbf{x}_j|^2)^{\frac{3}{2}}}. \quad (2.19)$$

This potential in equation (2.19) is called the softened point-mass potential (Binney and Tremaine, 1987, chap 2.8), because of the additional ϵ parameter. This parameter sets an upper limit for the force between two particles, which occurs at:

$$|\mathbf{x}_i - \mathbf{x}_j|^2 = \frac{1}{2}\epsilon^2 \quad (2.20)$$

and has magnitude of

$$2Gm^2 / (3^{\frac{3}{2}}\epsilon^2). \quad (2.21)$$

This chosen parameter ϵ enables us to give this upper limit, so that the force will not grow rapidly or reach infinity, when two point-masses approach or hit each other. If this force is too large, it will greatly increase the speed of the individual particle. We need smaller time steps to accurately calculate particles with higher velocities. So this limit is chosen so that time steps will be sufficiently small for high precision, but not too small. If time steps are smaller, the N-body simulation must evaluate longer. So we have to find a good equilibrium between precision and the speed of evaluation.

This approximation makes equation (2.19) unsuitable for simulation of individual stars, but can be used when particles represent groups of stars and are therefore well suited for galaxy simulations. We can make this assumption because the net force acting on a star in a galaxy is not determined by the force exerted by nearby stars, but rather by the whole structure of a galaxy. We call these models collisionless. The time it takes for one star to undergo a strong encounter with another star, called the relaxation time, is very long for galaxies. Therefore encounters in our models are not of any importance and we can use these approximations.

Dynamical friction

An important effect which becomes apparent, when doing a n-body simulations, is dynamical friction. It plays an important role when two galaxies are near each other or during a galactic merger. When an intruding galaxy passes by a region where another galaxy resides, a part of the mean forward motion of the intruding galaxy will be transferred to the random motion of individual particles. This effect slows down the galaxies and is called dynamical friction. A qualitative derivation of this effect is described in the book ‘Galactic Dynamics’ in paragraph 7.1 by Binney and Tremaine (1987). Chandrasekhar (1943) formulated a formula for

dynamical friction,

$$\frac{d\mathbf{v}_M}{dt} = -16\pi^2 \ln \Lambda G^2 m(M+m) \frac{\int_0^{v_M} f(v_m) v_m^2 dv_m}{v_M^3} \mathbf{v}_M \quad (2.22)$$

Where,

$$\Lambda \equiv \frac{b_{\max} V_0^2}{G(M+m)}. \quad (2.23)$$

This formula describes the decrease in speed, \mathbf{v}_M of a massive body with mass M while moving through a population of light particles with individual mass m , speed \mathbf{v}_m and velocity dispersion $f(\mathbf{v}_m)$. The parameter b_{\max} is the maximum value for the impact parameter b . The impact parameter is defined as the perpendicular distance between the velocity vector of a projectile and the center of the object it is approaching.

We use N-body simulations in our thesis to evaluate the dynamics of the Galaxy and M31.

2.4 Galactics

To model the Milky Way and Andromeda, we use the model built by Kuijken and Dubinski (1995). This model is called ‘‘Galactics’’ and produces reasonably stable and accurate axisymmetric N-body models for galaxies. This code is later improved by Widrow and Dubinski (2005). We used this improved version to model our galaxies. The reason we chosen this model, is that the model is built to fit observational data. For the MW these observations consist of surface brightness photometry, local stellar kinematics, the circular rotation curve and observations of dynamics of globular clusters and dwarf satellite galaxies. For other galaxies we have an ‘‘outside view’’ view which makes the observations more easy. The observational data which are used to fit the model are then mostly rotational velocity curves measured from HI gas kinematics. These models produce therefore accurate rotation curves. Other models, like the model of Cox and Loeb (2008), are based on more abstract hydrodynamical cosmological simulations. We believe that proper models should always have an observational basis.

Galactics produces a datafile containing a by us specified number of particles with mass, Cartesian coordinates and Cartesian velocity vectors per particle. These particles represent groups of stars. The number of represented stars depend on the mass of stars and the modeled galaxy. Galactics calculates all these parts, using fifteen user given parameters. In the analysis chapter we will discuss these parameters.

This model is an excellent tool for providing initial conditions for N-body simulations. Though it lacks the creation of important features such as globular clusters, gas dynamics and star formation. These would improve the level of realism.

| Physical quantity | Unit |
|-------------------|-----------------------------|
| Distance | kpc |
| Mass | $2.33 \cdot 10^9 M_{\odot}$ |
| Time | 9.78 Myr |
| velocity | 100 km/s |

Table 2.1: This table hold the units given by Galactics. We assume that $G = 1$.

Units of Galactics

Galactics uses the units in table 2.1 assuming that the gravitational constant, G , is 1. We will adopt these units in our thesis. In chapter A, in the appendix, the derivation is given for these units.

2.5 Nemo

NEMO is an extensible Stellar Dynamics Toolbox. This software consists of many useful programs for stellar dynamics. NEMO development started in 1986 in Princeton (USA) by Barnes, Hut and Teuben. We use this collection of applications to handle our data files. We use the folling programs

- **Snapmask** This program masks out certain particles while copying particles from an N-body systems. We use this program to make selections in our data files. We use it for instance to split data files into a Milky Way part and an Andromeda part.
- **Snapsort** This program is used to rearrange our data files. It can for instance sort particle on distance form center of density.
- **Hackdens** It calculates the local density in the configuration space using the hierarchical N-body algorithm. Using this program we can find the center of density of the system. This algorithm is based on the same method of our tree code, see chapter 2.6.
- **Snapradii** We used this program to find the Lagrangian radii of our two galaxies.

2.6 Simulations

We evaluate our N-body models using tree codes on computers with a graphics processing units (GPU). In this chapter we shortly discuss the advantages of tree codes and GPUs.

Tree codes

There are several ways to evaluate your n-body simulations. One could write a program which solves equation 2.19 for every time step. These types of programs are called direct integrators. The account of computations needed can be scaled with the number of particles in the evaluations. The computations needed increase as N^2 , with N as the number of particles. The number of computations scale directly with time.

We used an approximation in our integrator so that the needed computations now scale with $N \log N$. This approximation reduces the number of calculations in comparison with direct integrators. We use a tree code, which uses hierarchical force calculation algorithms. This method is based on the work by Barnes and Hut (1986).

This approximation incorporates the grouping of particles, which are then substituted by single pseudo particles. The three-dimensional space incorporating the model is divided hierarchically. This process continues to subdivide the model in such a way that each individual particle is isolated in their own subdivision or cell. In the next step the algorithm constructs a ‘tree of cells’. This is done by discarding the empty cells and accepting the cells with one occupant. This ‘tree’ has to be constructed each time step. Next some individually cells are grouped according to a criteria and form pseudo-particles. The last few steps are graphically shown in figure 2.1 for two dimensions. For final step the force on all (pseudo-)particles are calculated similar to a direct integrator. This is illustrated on the right of figure (2.1). This method can also be used in three dimensions and with objects with a complicated geometry, see figure 2.2.

The criteria mentioned above depends on the distance between particles and the size of the

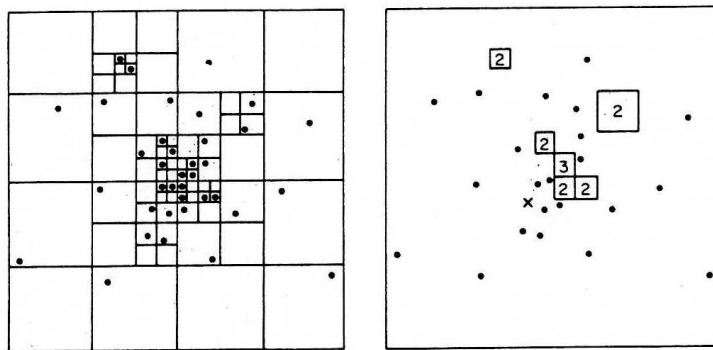


Figure 2.1: Hierarchical boxing and force calculation in two dimensions used in our tree code. On the left the area is subdivided in such a way that a minimal number of subdivisions are necessary to isolate each particle. On the right is shown how the force is calculated on particle x. Some particles are grouped together to form single pseudo particles. (Photo credit: Barnes and Hut (1986))

cells, so that

$$\frac{l}{D} < \theta. \quad (2.24)$$

With l defined as the length of each cell and D as the distance between the center of mass of the cell and the particle you calculate the force on. The opening angle, θ , is a value for the precision of the algorithm. The higher the opening angle, how faster the ‘tree’ is constructed each time step. This increases the error in your evaluation. Although tree codes are less precise than direct integrators, they perform excellent for collisionless systems. In our simulations we use

$$\theta = 0.5. \quad (2.25)$$

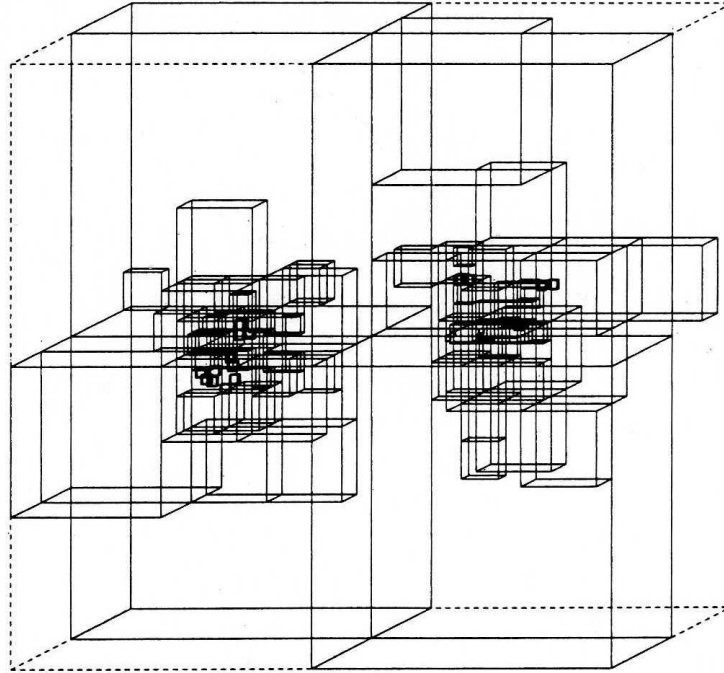


Figure 2.2: This figure shows a three-dimensional particle distribution. This particular image is taken from an encounter of two $N = 64$ systems. (Photo credit: Barnes and Hut (1986))

Nbint and Octagrav

We use the tree code, Octagrav, with force calculator, to evaluate our n-body simulation. This program is provided by Gaburov et al. (2008, in preparation). Octagrav makes use of GPUs. The simple leap-frog with fixed shared times-step integrator is provided by Harfst et al. (2008, private communication) and uses Octagrav.

The graphics processing unit, GPU

We used three dual core computers with NVIDIA 8800 GFX graphics cards (see figure 2.3) and a Linux architecture to evaluate our Nbody simulations. Two of them were provided by SARA Computing and Networking Services, Amsterdam.

The gaming industry has been developing high performance graphics card, with processors specially made to boost the frame rate of video games. These processors are programmable and can be used to evaluate N-body simulations. Nyland *et al.* (2004) first used commercial graphics processing units for N-body simulation. Portegies Zwart *et al.* (2007) compared these commercial cards from NVIDIA with the dedicated N-body simulation hardware called GRAPE (GRAvity PipE). These GRAPES are special purpose hardware integrators and are specialized in integrating $\text{constant}/r^2$. GRAPEs are still a bit faster and more accurate than a modern GPU. But they are outperformed by GPUs in their low cost, availability and larger memory. Recently NVIDIA brought a double precision GPU on the market, which has the potential to outperform the GRAPE in speed and accuracy. In our thesis we will use GPU's to do our simulations.



Figure 2.3: The NVIDIA 8800 GTX. One chip on this card is used to process our calculations. (Photo credit: NVIDIA Corporation)

CHAPTER 3

Initial Conditions

In this section we will give an overview of the properties of the Milky Way and M31 found in the literature. We use these properties to find the initial conditions for our models. For the individual galaxies we will predominately use the paper from Widrow and Dubinski (2005) as a guideline. The authors of this paper created a model for galaxies using galactic rotation curves. Again, we favor this approach, because of its observational basis. Other papers, like the paper of Cox and Loeb (2008), use the cosmological simulations as their basis. For the interaction between M31 and the MW we will mostly use the initial conditions given in the paper from van der Marel and Guhathakurta (2008).

3.1 Initial conditions of the Milky Way and Andromeda

The sixteen parameters of Galactics are typically poor constrained. The parameters in table (3.1) are chosen, so that the produced rotation curve fits the observed one and certain theoretical considerations are met.

The model is based on some assumptions. First, the model is axisymmetric in the z-axis. Most galaxies exhibit non-axisymmetric phenomena, such as central bars and spiral arms. However, these models are subject to non-axisymmetric instabilities which can evolve in the N-body simulation. Second, the assumption is made that galaxies only comprise of three components, disk, bulge and halo. This excludes globular clusters and stellar halos. Third, these models assume an isotropic velocity distribution. Fourth, the most severe assumption is that this model only uses collisionless particles, whereas a substantial part of the disks mass is in gas. Fifth, although this model can incorporate a super massive black hole in the center of the galaxy, we disable this feature. This black hole only has a significant influence on the very most center of the galaxy and is not relevant for our purpose. The effect of the black hole on the relative gravitational potential is:

$$\phi^*(r) = \phi(r) + \frac{M_{BH}}{r} \tag{3.1}$$

| Parameter | Description | Milky Way | Andromeda | Units |
|------------------|------------------------------------|-----------|-----------|---------------------------|
| σ_h | Halo characteristic velocity | 2.496 | 3.371 | 100 km s ⁻¹ |
| a_h | Halo scale length | 12.96 | 12.94 | kpc |
| α_h | Halo cut-off parameter | 0.83 | 0.75 | - |
| M_d | Disk Mass | 19.66 | 33.40 | $2.33 \cdot 10^9 M_\odot$ |
| R_d | Disk scale length | 2.806 | 5.577 | kpc |
| R_{out} | Disk truncation radius | 30 | 30 | kpc |
| δR_{out} | Sharpness of truncation | 1.0 | 1.0 | - |
| h_d | Disc scale height | 0.409 | 0.3 | kpc |
| σ_{RO} | Radial velocity dispersion at GC | 0.7 | 0.8 | 100 km s ⁻¹ |
| R_σ | Scale length for radial dispersion | 2.806 | 5.577 | kpc |
| a_b | Bulge scale length | 0.788 | 1.826 | kpc |
| α_b | Bulge cut-off parameter | 0.787 | 0.929 | - |
| M_{BH} | Mass of central black hole | 0 | 0 | $2.33 \cdot 10^9 M_\odot$ |

Table 3.1: Galactics parameters for the MW and M31 (Widrow and Dubinski, 2005). The units are chosen, so that $G = 1$.

In the model the black hole only influence the potential of the system. It is not represented by a particle. Therefore it is not usable in our evaluation.

Now we shall qualitatively describe all Galactics parameters. The halo is defined by three free parameters and some dependent parameters. The halos' radius is cut-off by α_h , the density is defined by a_h , the particle velocities by σ_h . Notice that the halos mass is not a free parameter, but completely depends on other parameters like M_d . The parameters R_d , R_{out} , δR_{out} and h_d describe the disk's geometry and M_d is its mass. Notice again that this is the only free parameter which contains mass. The bulges' cut-off and density are parameterized as a_b and α_b . Because we do not use the super massive black hole feature in the model, the M_{BH} equals 0. Galactics produces data files with mass, position and velocity columns. In figure (3.1), an example is given of the first few lines of a Galactics output file.

3.2 Parameter study of the Milky Way Andromeda system

The parameters given in chapter 3.1 provide the initial conditions, which result from fits to observations. However for our parameter study we must change some parameters so that both systems will increase or decrease mass. We do this by changing the parameters of both halos. We need to increase both systems mass by 30 percent for some models. We do this by increasing the velocities in the halo, by changing the a_h parameter in Galactics. The velocities increase when the gravitational potential is increased. Potential is dependent of mass, so mass of the halo will increase. The change of mass of the halo has some influence on the mass and size of the disk and bulge. It also influences the size of the halo. This can be stopped

```

70000
1.51339069e-03 -3.08295727e+00 -4.32949543e+00 6.86662018e-01 1.94243932e+00 -1.27536809e+00 -1.97001666e-01
1.51339069e-03 -1.67908037e+00 -3.09025586e-01 3.22072208e-01 6.84477985e-01 -1.92960441e+00 -1.54821694e-01
1.51339069e-03 5.29213142e+00 1.29490292e+00 5.76239645e-01 -5.70469677e-01 2.26985025e+00 -4.45173681e-02
1.51339069e-03 -9.45444584e+00 -7.77926922e+00 5.80890357e-01 1.38757801e+00 -1.92830193e+00 -5.82336746e-02
1.51339069e-03 -9.12416649e+00 -4.98375273e+00 -7.70067751e-01 1.07484734e+00 -1.95747006e+00 -2.73859929e-02
1.51339069e-03 -2.04251409e+00 1.42651784e+00 -6.01165295e-01 -9.21870112e-01 -2.13667274e+00 9.77174863e-02
1.51339069e-03 -3.01448941e+00 6.18614674e+00 -6.46427393e-01 -1.99767900e+00 -8.83552074e-01 9.41213071e-02
1.51339069e-03 -4.21747732e+00 -2.48310542e+00 2.50820249e-01 1.09763038e+00 -1.57110500e+00 -7.65016973e-01
1.51339069e-03 -3.51872301e+00 -1.47662258e+00 -4.44473237e-01 8.06781292e-01 -1.94767296e+00 2.52615482e-01

```

Figure 3.1: This is an example of the first lines of a Galactics output file. The first line is the header. The header contains a number with the total amount of particles. Each following line describes parameters of each particle. The first column is the mass. The second to fourth column are the Cartesian x , y and z coordinates. The last three columns are the Cartesian velocity components V_x , V_y and V_z . The mass is in $2.33 \cdot 10^9 M_\odot$. Length and velocity are in kpc and 100 km s^{-1} .

by changing the halo cut-off parameter, α_h . So to increase the total mass, we must tune or “tweak” the system. We did this by trial and error. The resulting systems disk and bulge have similar size and relative mass as the Milky Way and Andromeda Galaxy. However the resulting rotational curve is different for these systems.

We use the same recipe to create systems with a larger and smaller halo radius by changing a_h and α_h . The individual properties of these four galaxies can be found in table B.2, B.3, B.4 and B.5.

3.3 Initial conditions of the Milky Way Andromeda system

For processing we must edit the M31 Galactics output files. We want to rotate and translate it. Also we must add the velocity components of M31 to these files. In the next few paragraph we will show how you can do that. In table (3.2) all the parameters are shown, which we need to set-up the MW-M31 system. Also in table (3.2) are the sources in the literature we used. We adopt a Cartesian coordinate system, (x,y,z) , for the position and velocity as postulated by van der Marel and Guhathakurta (2008), with origin in the Galactic center. The z -axis points toward the the Galactic north pole, the x -axis points in the direction from the Sun towards the Galactic center and the y -axis points in the direction of the Suns rotation in the Galaxy.

Rotation

Andromeda’s spin axes is not parallel to the the Milky Way’s. So before we translate M31 to the proper coordinates, we have to rotate it. We can rotate Andromeda using equation

$$\mathbf{r}_{M31} = \mathbf{R}_{M31} \mathbf{r}. \quad (3.2)$$

| Parameter | | Source in Literature |
|--------------------------------|----------------------------------|---------------------------------------|
| Distance Sun - M31 | 770 | McConnachie and Irwin (2006) |
| Distance Sun - Galactic Center | 8.5 | Kerr and Lynden-Bell (1986) |
| Orientation spin axis M31 | $39.8^\circ, 77.5^\circ$ | de Vaucouleurs (1958) |
| Position M31 | -379.2, 612.7, -283.1 | van der Marel and Guhathakurta (2008) |
| Position M31 RA | $00^{\text{h}}42^{\text{m}}44.3$ | NASA/IPAC Extragalactic Database |
| Position M31 dec | $+41^\circ 16' 09.4''$ | NASA/IPAC Extragalactic Database |
| Radial Velocity M31 | 117 | Courteau and van den Bergh (1999) |
| Transverse Velocity M31 | 42 | van der Marel and Guhathakurta (2008) |

Table 3.2: In this table the properties of the MW-M31 system are shown and the corresponding sources in the literature. The distance is measured from the Galactic center to the center of Andromeda in kpc. The orientation of the spin axis is given in the equatorial coordinate system and the position is given in Cartesian coordinates. All values in this table are galactocentric except for the heliocentric orientation of Andromeda’s spin axis. The units of both velocities are given in (km s^{-1}) .

with,

$$\mathbf{R}_{\text{M31}} = \begin{pmatrix} 0.7703 & 0.3244 & 0.5490 \\ -0.6321 & 0.5017 & 0.5905 \\ -0.0839 & -0.8019 & 0.5915 \end{pmatrix} \quad (3.3)$$

and \mathbf{r}_{M31} and \mathbf{r} as the rotated and unrotated position and velocity vectors of Andromeda. We can multiply the rotation matrix, R , with the position vector, (x,y,z) , and the velocity vector (V_x, V_y, V_z) in the Galactics output data file. The full derivation of this rotation matrix can be found in chapter A in the appendix.

Translation

Now the orientation of Andromeda is taken care of, we can translate Andromeda to the correct coordinates using position vector

$$\mathbf{P} \equiv (-379.2, +612.7, +283.1). \quad (3.4)$$

This vector is the Cartesian position vector of M31 with its origin the the Galactic center. Its units are kpc. When we want to translate M31 we have to add the vector \mathbf{P} to the x , y and z column in then Galactics datafile.

Adding of transverse and radial velocities

To add the radial velocity component to M31 we have to add vector \mathbf{V}_{rad} to the M31 velocity vectors in the Galactics datafile. We first find the opposed unit vector of the position vector,

$$\mathbf{P} \equiv (-379.2, +612.7, +283.1), \quad (3.5)$$

$$-\hat{\mathbf{P}} = \frac{-\mathbf{P}}{|\mathbf{P}|}, \quad (3.6)$$

$$-\hat{\mathbf{P}} = (+0.4898, -0.7914, +0.3657). \quad (3.7)$$

Now we can multiply this vector with the observed radial velocity,

$$\mathbf{v}_{\text{rad}} = -\hat{\mathbf{P}}117 \text{ km s}^{-1} \quad (3.8)$$

As a final step we add the vector \mathbf{v}_{rad} to the velocity vectors in the Galactics datafile.

To find the transverse velocity component we first choose an arbitrary vector, \mathbf{A} . We choose an arbitrary vector, equation (3.9) on the assumption that its direction does not influence the outcome of our simulations. It will effect, however, the shape of the tidal features, while merging.

$$\mathbf{A} \equiv (x, 1, 1) \quad (3.9)$$

which have to be perpendicular to vector \mathbf{P} . This vector can be found by taking the in-product,

$$-\hat{\mathbf{P}} \cdot \mathbf{A} = 0. \quad (3.10)$$

This gives us a value for x and by solving,

$$\hat{\mathbf{A}} = \frac{\mathbf{A}}{|\mathbf{A}|}, \quad (3.11)$$

a value for $\hat{\mathbf{A}}$. Plugging in the numbers we get,

$$x = 0.8691, \quad (3.12)$$

$$\hat{\mathbf{A}} = (0.5236, 0.6024, 0.6024). \quad (3.13)$$

Now we can calculate the transverse speed component $\mathbf{v}_{\text{trans}}$,

$$\mathbf{v}_{\text{trans}} = 42 \text{ km s}^{-1} \hat{\mathbf{A}}. \quad (3.14)$$

This component must be added to the velocity of Andromeda in the datafile. We also vary this component by multiplying it with some factors. For our parameter study we use the factors 0, 0.5, 0.8, 1 and 1.2.

Centering the system

Now as last step we put the the origin of the datafile in the center of mass. This step helps us analyze the data more easily. A potential merger will therefor happen in the proximity of coordinate (0, 0, 0). We use Nemo to put the origin in the center of mass.

CHAPTER 4

Results

In this chapter we will discuss the results of our thesis. Table 4.1 contains all the models we evaluated. We first checked if the models of the individual galaxies were stable. Then we made a test run of our Milky Way Andromeda system. The influence of the number of particles, N , is investigated in models Mn1 to Mnv1. Then we evaluated the system with different transverse velocities in models Mv1 to Mv1.2. Finally we evaluated the system for different total mass and halo radius of Andromeda in models Mm1.3V0 to Mr100v1.2. Some models we converted all time steps to video format.

4.1 Galactics

We used Galactics to produce both Andromeda and the Milky Way galaxy. In table 4.2 the properties are given for both systems. In table B.2, B.3, B.4 and B.5 the properties are shown for our models, we made for the parameter study. Notice that these radii and masses are produced by the thirteen parameters in table 3.1. The total masses and disk masses of the Milky Way and Andromeda produced by Galactics with our initial conditions are

$$M_{\text{tot,MW}} = 78 \cdot 10^{10} M_{\odot}, \quad (4.1)$$

$$M_{\text{d,MW}} = 3.53 \cdot 10^{10} M_{\odot} \quad (4.2)$$

and

$$M_{\text{tot,M31}} = 68 \cdot 10^{10} M_{\odot}. \quad (4.3)$$

$$M_{\text{d,M31}} = 8.0 \cdot 10^{10} M_{\odot}. \quad (4.4)$$

$$(4.5)$$

Notice that Andromeda's disk is more massive than the Milky Ways, but the total mass is less massive.

| Name | N | System | $\mathbf{v}_{\text{trans}}$ | M_{tot} | $R_{\text{h,M31}}$ | video |
|-----------|---------|--------|-----------------------------|------------------|--------------------|-------|
| Mmw | 350,000 | MW | - | - | - | yes |
| Mm31 | 350,000 | M31 | - | - | - | yes |
| Mtest1 | 70,000 | MW-M31 | 1 | 1 | 201 | yes |
| Mn1 | 70,000 | MW-M31 | 1 | 1 | 201 | yes |
| Mn2 | 140,000 | MW-M31 | 1 | 1 | 201 | no |
| Mn3 | 280,000 | MW-M31 | 1 | 1 | 201 | no |
| Mn4 | 560,000 | MW-M31 | 1 | 1 | 201 | no |
| Mv1 | 700,000 | MW-M31 | 1 | 1 | 201 | yes |
| Mv0 | 700,000 | MW-M31 | 0 | 1 | 201 | yes |
| Mv0.5 | 700,000 | MW-M31 | 0.5 | 1 | 201 | yes |
| Mv0.8 | 700,000 | MW-M31 | 0.8 | 1 | 201 | yes |
| Mv1.2 | 700,000 | MW-M31 | 1.2 | 1 | 201 | no |
| Mm1.3v0 | 700,000 | MW-M31 | 0 | 1.3 | 201 | no |
| Mm1.3v0.8 | 700,000 | MW-M31 | 0.8 | 1.3 | 201 | no |
| Mm1.3v1 | 700,000 | MW-M31 | 1 | 1.3 | 201 | no |
| Mm1.3v1.2 | 700,000 | MW-M31 | 1.2 | 1.3 | 201 | no |
| Mm0.7v0 | 700,000 | MW-M31 | 0 | 0.7 | 201 | no |
| Mm0.7v0.8 | 700,000 | MW-M31 | 0.8 | 0.7 | 201 | no |
| Mm0.7v1 | 700,000 | MW-M31 | 1 | 0.7 | 201 | no |
| Mm0.7v1.2 | 700,000 | MW-M31 | 1.2 | 0.7 | 201 | no |
| Mr350v0 | 700,000 | MW-M31 | 0 | 1 | 350 | no |
| Mr350v0.8 | 700,000 | MW-M31 | 0.8 | 1 | 350 | no |
| Mr350v1 | 700,000 | MW-M31 | 1 | 1 | 350 | no |
| Mr350v1.2 | 700,000 | MW-M31 | 1.2 | 1 | 350 | no |
| Mr100v0 | 700,000 | MW-M31 | 0 | 1 | 100 | no |
| Mr100v0.8 | 700,000 | MW-M31 | 0.8 | 1 | 100 | no |
| Mr100v1 | 700,000 | MW-M31 | 1 | 1 | 100 | no |
| Mr100v1.2 | 700,000 | MW-M31 | 1.2 | 1 | 100 | no |

Table 4.1: This table is an overview of all models we carried out for this thesis, with their main characteristics. Where N is the number of particles and $\mathbf{v}_{\text{trans}}$ and M_{tot} are the fractions of the transverse velocity of Andromeda of 42 km/s the total mass of the system. The halo radius is given in kpc. All models were evaluated for 900 time steps, which corresponds with almost 9 Gyr. Some models are converted to video. The last column shows which models we converted.

| Parameter | Milky Way | Andromeda | Total system |
|--------------------------------|------------|------------|--------------|
| Galactics Model | MWb | M31a | Mv1 |
| Number of particles, N | 350,000 | 350,000 | 700,000 |
| Total Mass | 335.232666 | 293.737518 | 628.97018 |
| Disk Mass | 15.1457396 | 34.1285782 | - |
| Bulge Mass | 5.10096455 | 12.3888931 | - |
| Halo Mass | 314.985962 | 247.220047 | - |
| Disk Edge | 32 | 32 | - |
| Bulge Edge | 3.05999994 | 8.05999947 | - |
| Halo Edge | 244.48999 | 201.619995 | - |
| $M_{\text{MW}}/M_{\text{M31}}$ | - | - | 1.1412661 |

Table 4.2: This table contains the mass and radii for the two models we created using Galactics for the initial conditions. Notice that although Andromeda’s disk is more massive than the Milky Way’s, its total mass is less massive. The units of the mass and the radii are $2.33 \cdot 10^9 M_{\odot}$ and kpc.

The rotation curve

Figure 4.1 shows the rotational curve of the model of Andromeda produced by Galactics. Also plotted is observational data by Kent *et al.* (1989) and Braun (1991). The rotation curve of the model of the Milky Way can be found in figure 4.2. This plot corresponds with observations by Binney and Dehnen (1997) and Levine *et al.* (2008).

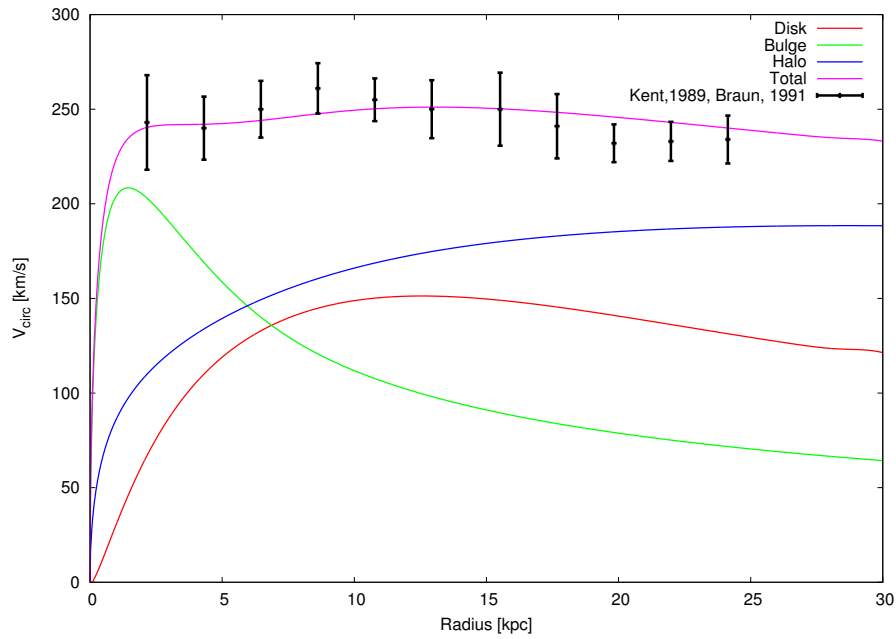


Figure 4.1: This plot shows the rotational speed curve of our model of the Andromeda Galaxy and the observational data form Kent *et al.* (1989) and Braun (1991). This data is taken form model Mm31, $N = 350,000$.

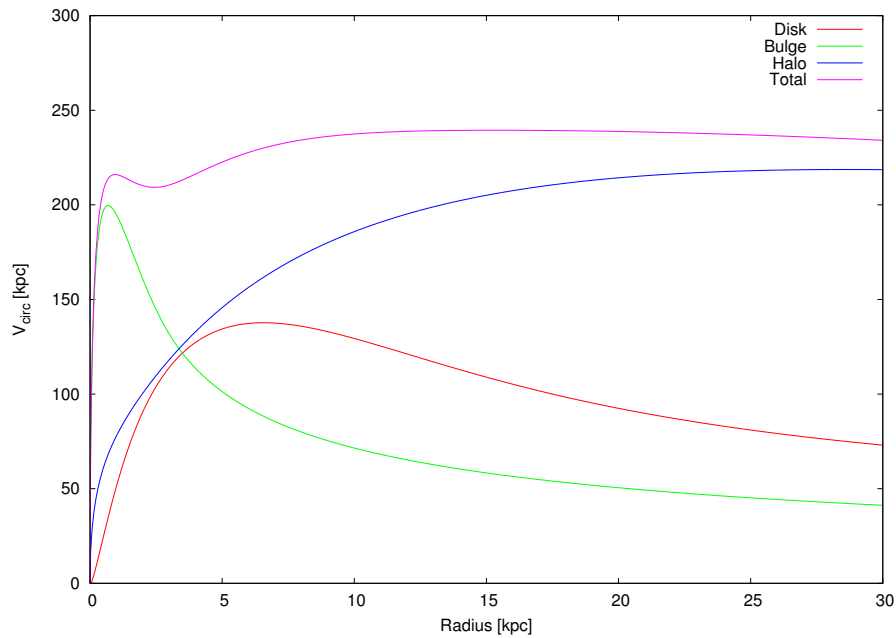


Figure 4.2: This plot shows the rotational velocity curve of our model of the Milky Way, which corresponds with observational data form Binney and Dehnen (1997) and Levine *et al.* (2008).

Stability

We use the change in radii of the disk as an instrument to determine if the models are stable. The radii do not change much of the unperturbed systems, see figure 4.3. This means that both systems are stable. The model of Andromeda is more stable then the model of the Milky Way. Milky Ways radii change more over time then Andromeda's. Both plots show signs of osculations in the upper radii. These variations correspondent with the creation of spiral arms.

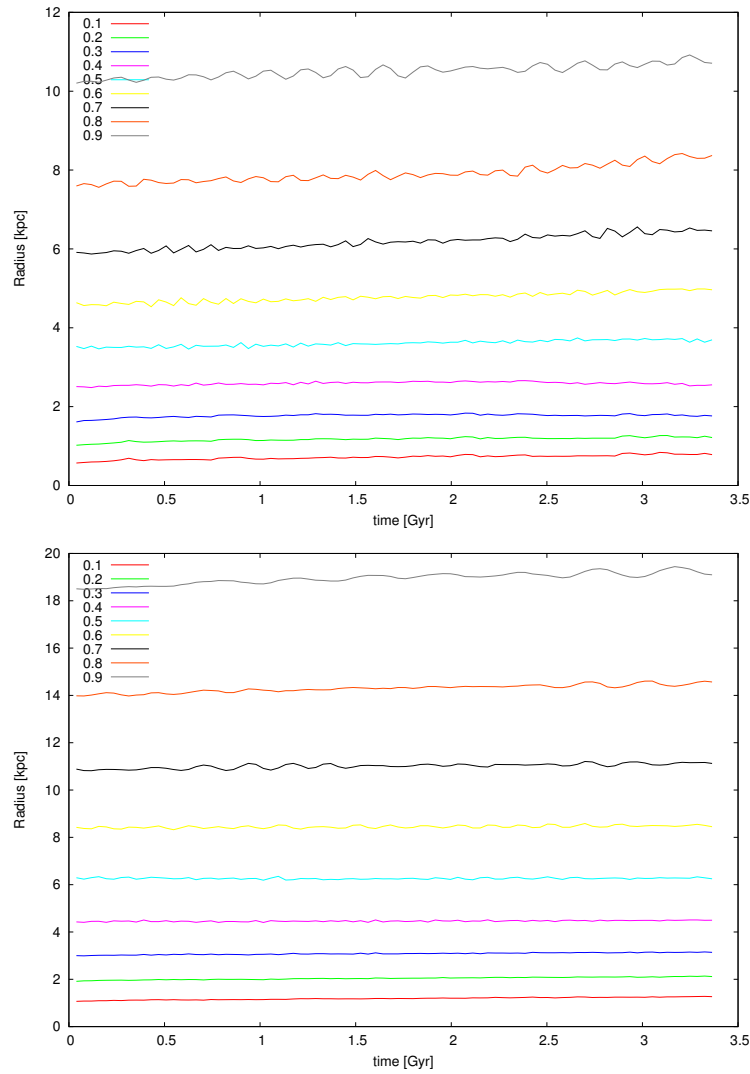


Figure 4.3: These plots show the radii of the Milky Way (top) and Andromeda (bottom) in terms of different mass fractions of the disk and bulge. At radius $R = 0.1$, ten percent of all mass of the disk and bulge are within this radius, and so on. The data for these plots is taken from model Mmw and Mm31. It shows that the radii do not change much over time, and that therefore the system is considered stable. The upper three line show harmonic features. They correspond with the formation of spiral arms and bars.

The formation of spiral arms is demonstrated in figure 4.4 and 4.5. The Milky Way in our model develops a bar, see figure 4.6. In these figures the yellow dots represent density. The increasing size and color corresponds with an increase of density.

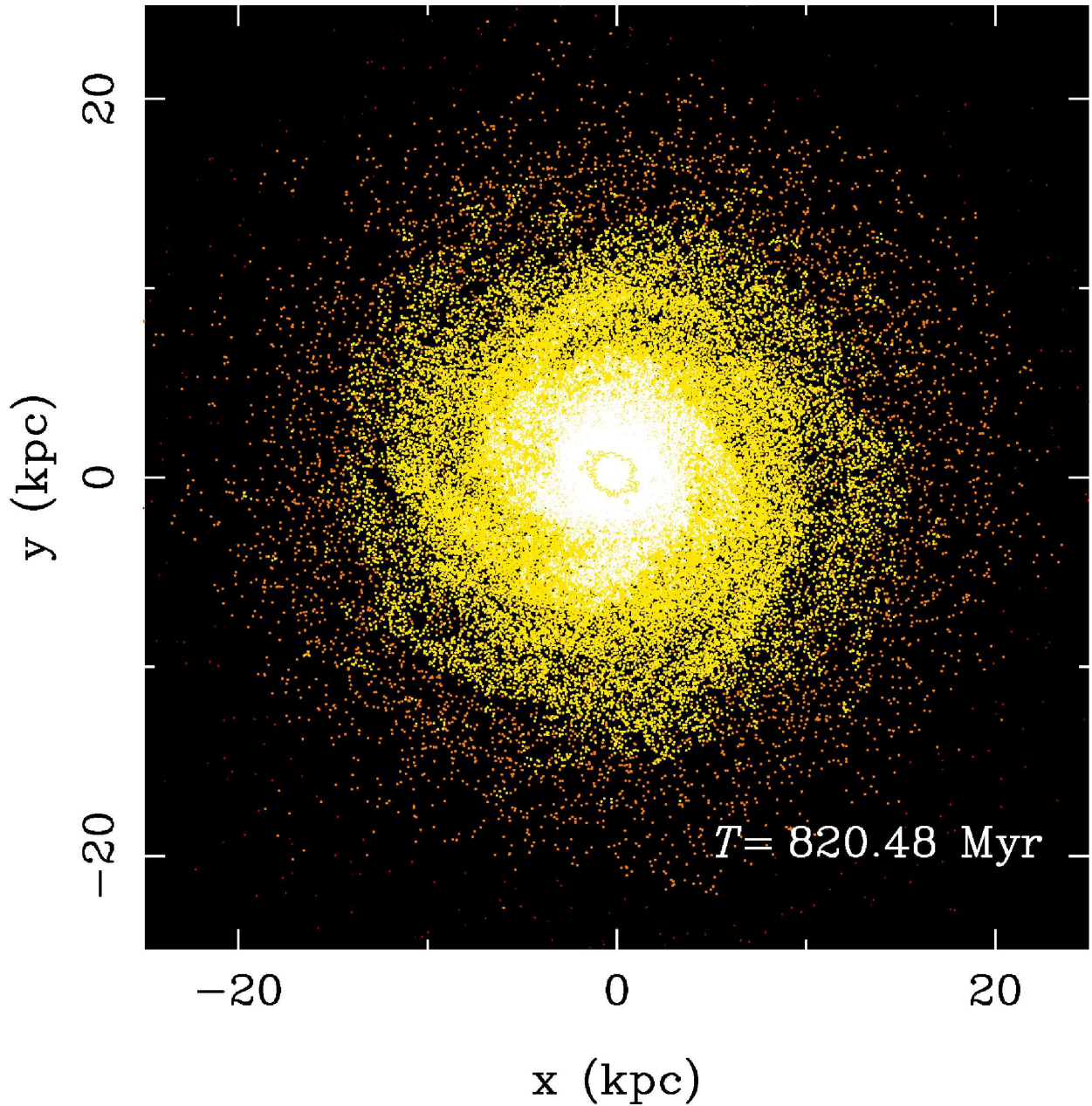


Figure 4.4: This figure shows a snapshot from the evaluation of the model of the Milky Way, Mmw, at time 820.48 Myr. This snapshot shows the appearance of spiral features. The yellow dots represent density. The increasing size and and intensifying color corresponds with an increase of density.

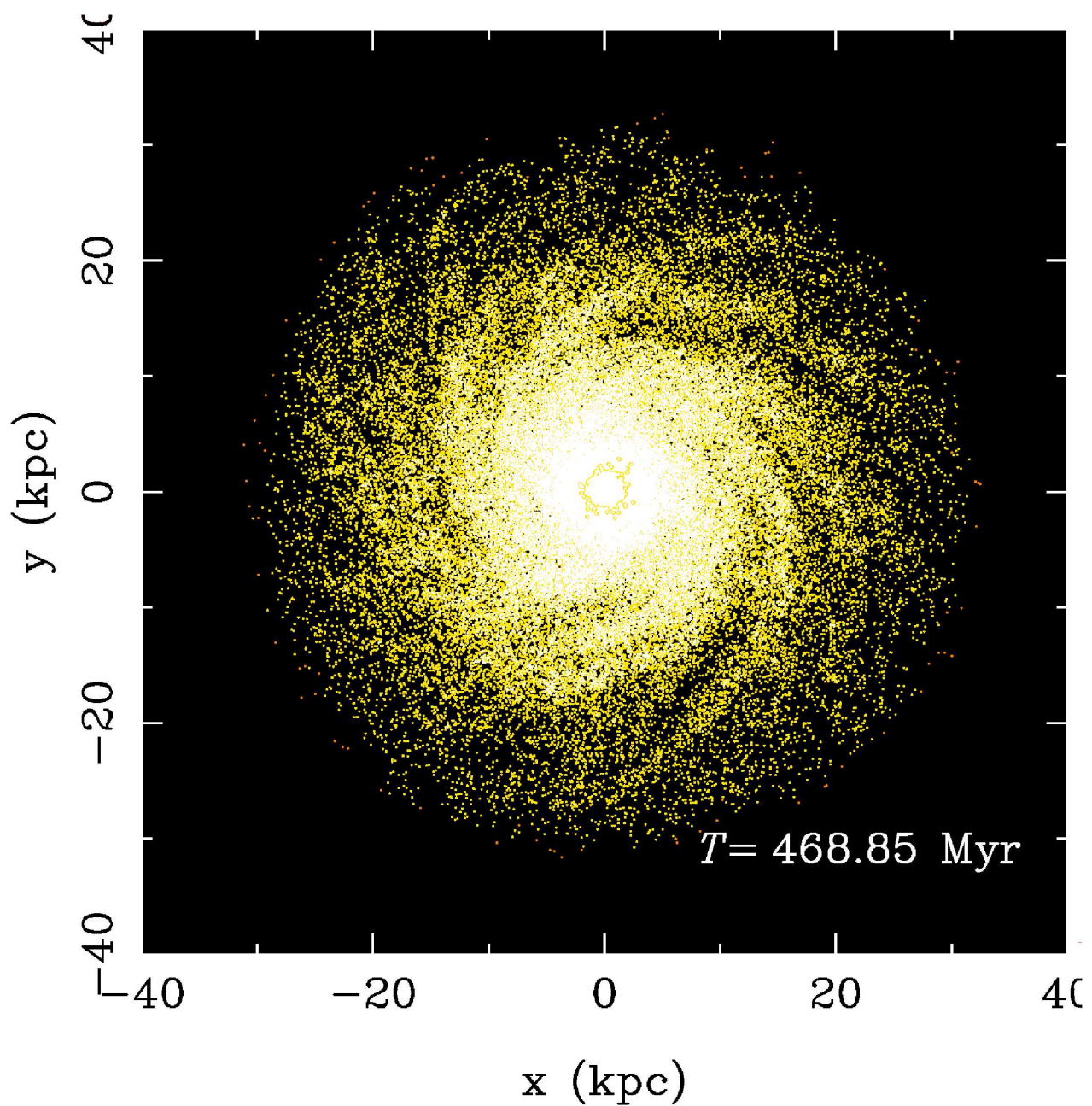


Figure 4.5: This figure shows a snapshot from the evaluation of the model of Andromeda, Mm31, at time 468.85 Myr. This snapshot shows the appearance of spiral features. The yellow dots represent density. The increasing size and intensifying color corresponds with an increase of density.

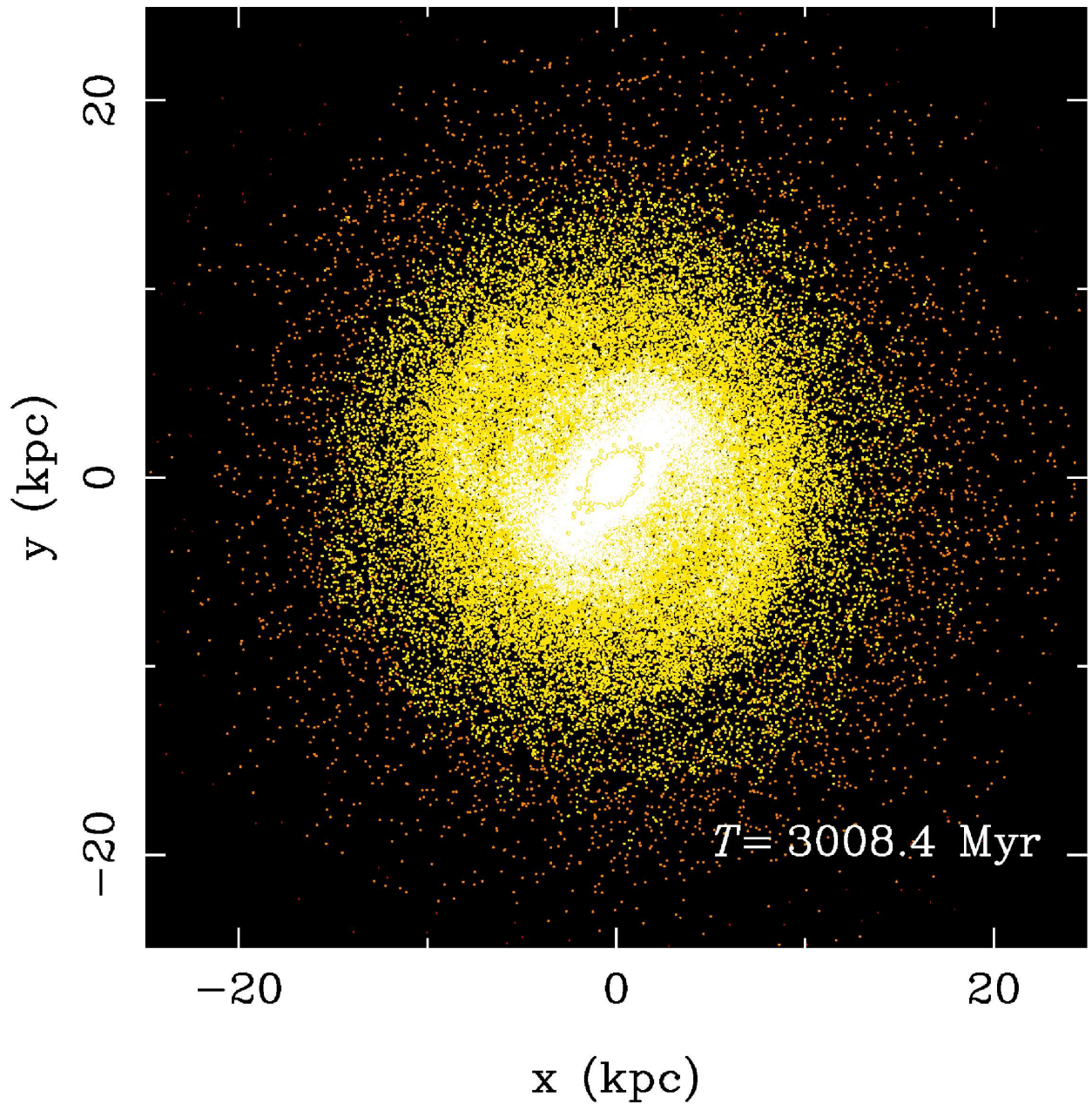


Figure 4.6: This figure shows a snapshot from the evaluation of the model of the Milky Way, Mmw, at time 3008.4 Myr. This snapshot shows the appearance of spiral features and the formation of a bar in the systems center. The yellow dots represent density. The increasing size and and intensifying color corresponds with an increase of density.

The leading theory on the formation of spiral arms was postulated by Lin and Shu (1964). They argued that spiral arms are manifestations of spiral density waves, caused by orbits of the disk stars. They assume stars travel in elliptical orbits. Those orbits are correlated to each other and vary in a smooth way with increasing radius. The orbits resonate and this gives the effect of spiral arms. Our models start axis-symmetric. That means that all objects have circular orbits. After a few time steps the spirals arms appear in our models. This would mean that the orbits of stars are perturbed, getting more eccentric and heat up the disk. The process which causes this, is called swing amplification (Toomre, 1981). This would imply that our modeled disks are unstable in nature. A recent paper by Seigar *et al.* (2008) shows a correlation between the formation of spirals and the perturbations caused by the super massive black hole in a galactic center. The creation of the bar in the modeled Milky Way is also caused by the transfer of angular momentum from the disk stars. This also implies an unstable disk. These instabilities have no influence on our experiments and are not considered to be problem. We use the vertical scale height as an indicator of disk stability. Figure 4.7 shows the variability of the average height above midplane for every disk particle. Again notice that the scale height of the disk Andromeda is more stable, then the scale height of the disk of the Milky Way. Both disks remain flat during our simulations and do not expand much in the vertical direction. Another way to look into the stability of a rotating disk is to determine Toomre's stability criterion. This criterion is defined by Toomre (1964) as

$$Q \equiv \frac{\sigma_R \kappa}{3.36 G \Sigma} > 1 \quad (4.6)$$

In this equation σ_R is the radial velocity dispersion, κ is the epicycle frequency, G is the gravitational constant and Σ is the surface density of the disk particles. All values larger than one are considered stable. We can use this number as a thermometer for galactic disks. The value increases with dispersion in the disk. If there is a high value of dispersion, the disk is then considered warm. In figure 4.8 we have plotted the values of Q in our disks. It shows us that both disks are stable, but that the Milky Way has a higher velocity dispersion. Therefore the disk of the Milky Way is warmer, than Andromeda's disk.

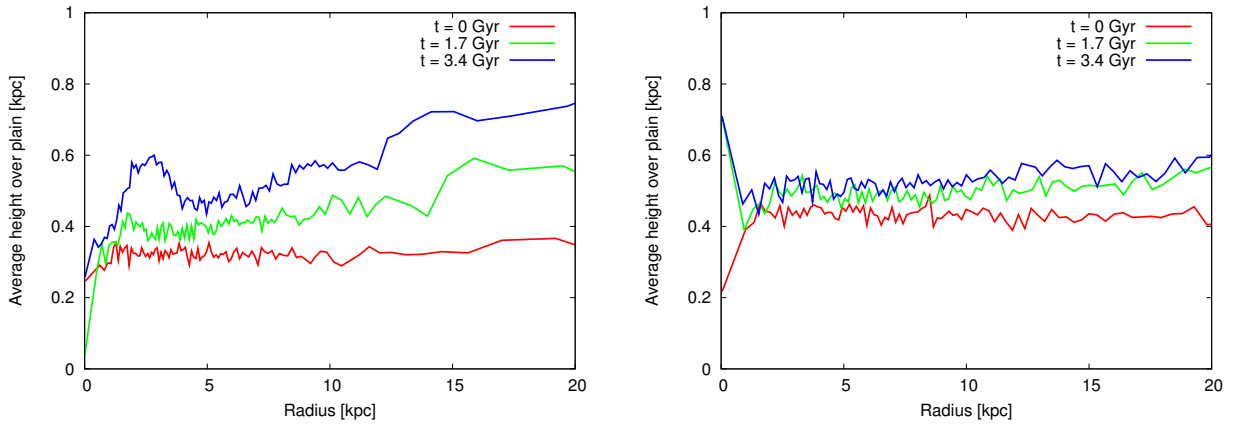


Figure 4.7: These two plots show the average height of every disk particle above galactic midplane for the disk radius. The three lines represent different times.

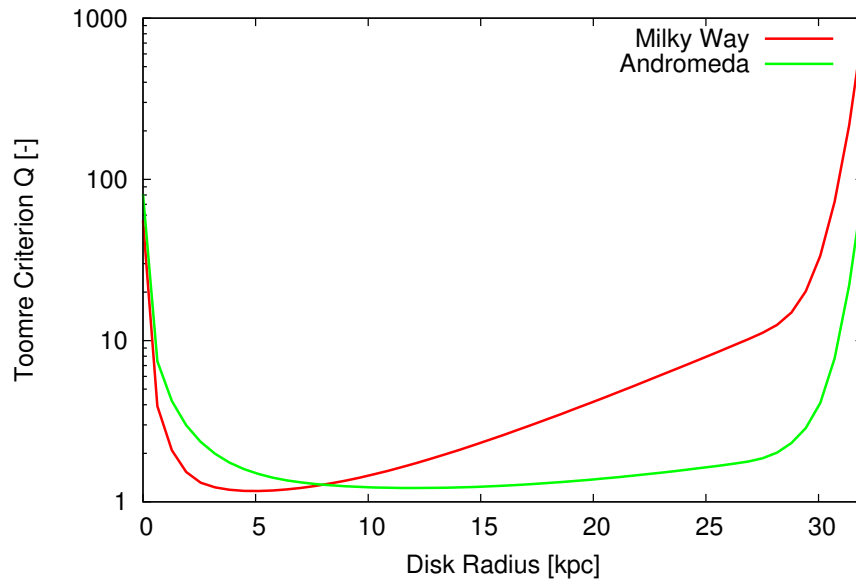


Figure 4.8: This plot shows the Toomre stability criterion plotted versus radius of the disk.

Particle numbers

We can choose the number of particles, N and this numbers influence the simulation. In figure 4.9 the effect of N on the simulations is plotted. The difference between particle numbers, $N = 70,000$, and $N = 700,000$ is marginal. It starts to play a small role at the end of the simulation, at $t = 8$ Gyr. All our simulations run at $N = 700,000$ to $t = 9$ Gyr.

In figure 4.10 the relative error in the total energy is plotted for different values of N . We define this relative error as

$$\chi(t) \equiv \frac{E_{\text{tot}}(0) - E_{\text{tot}}(t)}{E_{\text{tot}}(t)}. \quad (4.7)$$

Where $E_{\text{tot}}(0)$ is the total energy of the system at the start of the simulation and $E_{\text{tot}}(t)$ is the total energy at time, t . The relative error increases when when N is decreased. Most of are simulations have $N = 700,000$. The relative error at this N is at the end, $\chi(9) = 1.73794 \cdot 10^{-05}$. This is a small number, which means that the total energy in our simulations does not change much over time. This result can be interpreted as proof that our simulations have high precision.

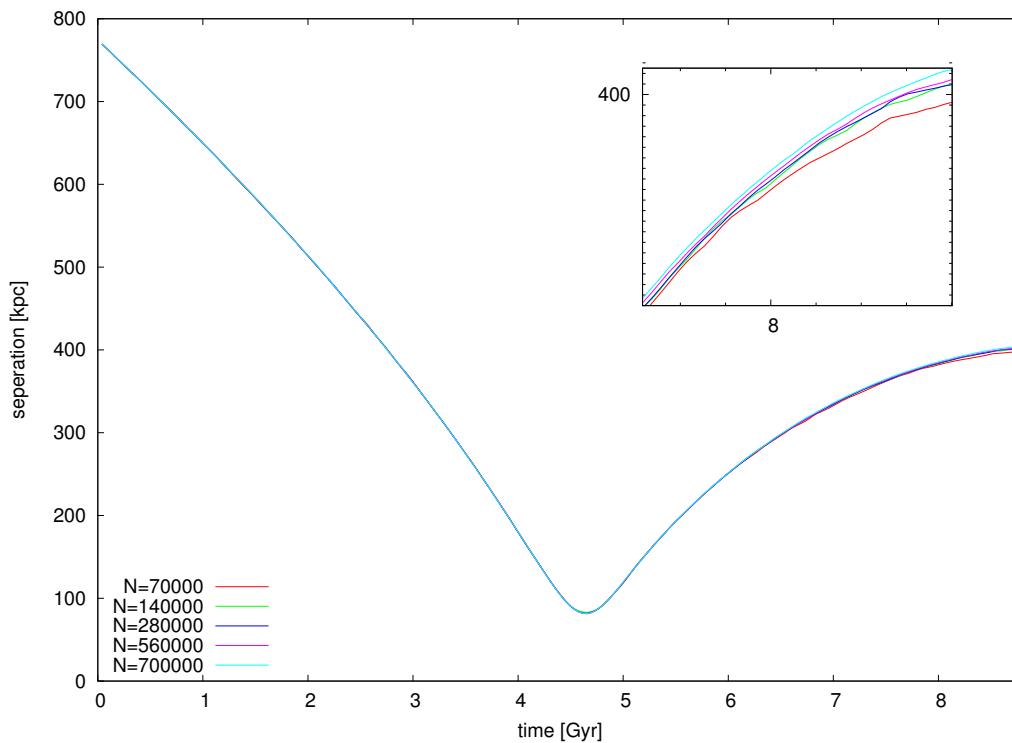


Figure 4.9: This plot shows the separation of M31 and the Milky Way evolving over time for different number of particles. This data is taken from models Mn1, Mn2, Mn3, Mn4 and Mv1.

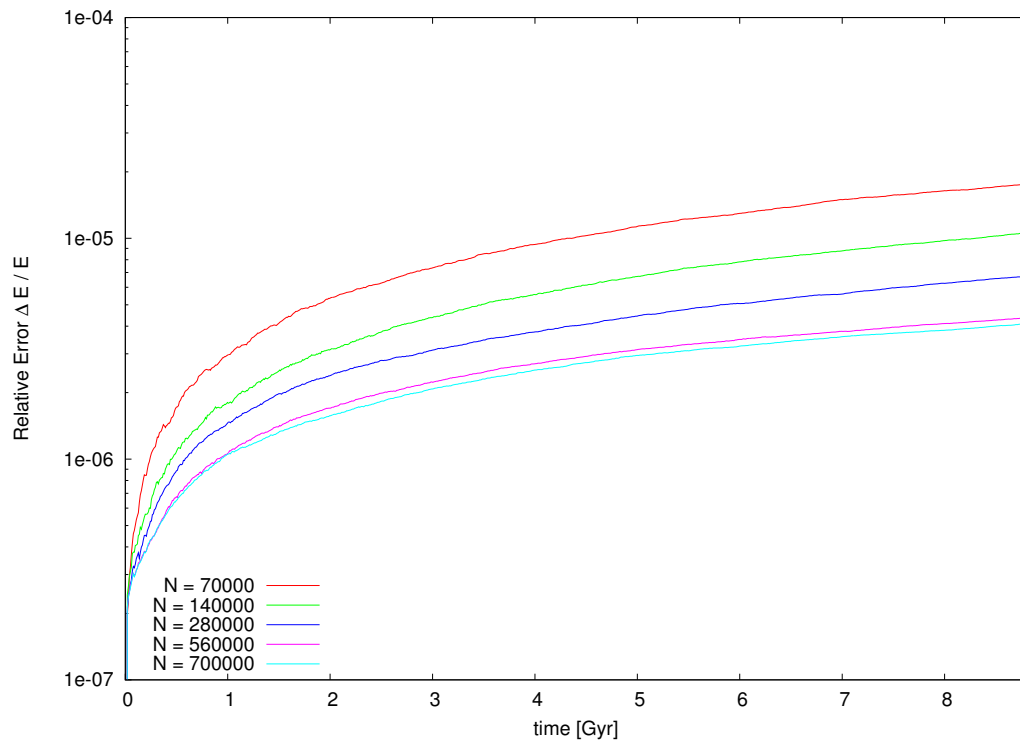


Figure 4.10: This plot shows the relative error as defined in equation (4.7) versus simulated time.

4.2 Separation versus Time

We plot the separation between the Milky Way and Andromeda versus time. This is a useful tool to visualize the dynamics of the Milky Way Andromeda system. We define separation as the distance between the two centers of density of both systems. Under these circumstances it is better to choose the center of density instead of the center of mass. The center of mass can move rapidly during a merger event, due to formation of non-symmetric phenomenon like tidal tails. While the center of mass is more stable during possible merger events. The evolution of the separation is plotted in figure 4.11. Every line represents a different transverse velocity, $\mathbf{v}_{\text{trans}}$. We define the first minimum in figure 4.11 as moment of first approach, second minimum as moment of second approach, and the third minimum as moment of merger. We notice that these first and second moments of approach happen at various separations.

Transverse velocity

To examine the effect of the magnitude of the transverse velocity component of the relative velocity of Andromeda, we evaluated the Milky Way Andromeda system with five different velocities, which range from, $\mathbf{v}_{\text{trans}} 0$ km/s to $\mathbf{v}_{\text{trans}} = 50.4$ km/s. The results of evaluation are plotted in figure 4.11 and 5.1. In the situation of $\mathbf{v}_{\text{trans}} = 0$ the galaxies collide at $t \approx 4.2$ and are fully merged at $t \approx 5$. When we increase $\mathbf{v}_{\text{trans}}$ the merger will happen later in time. For velocities of, $\mathbf{v}_{\text{trans}} 42$ km/s and larger, only the moment of first approach is visible.

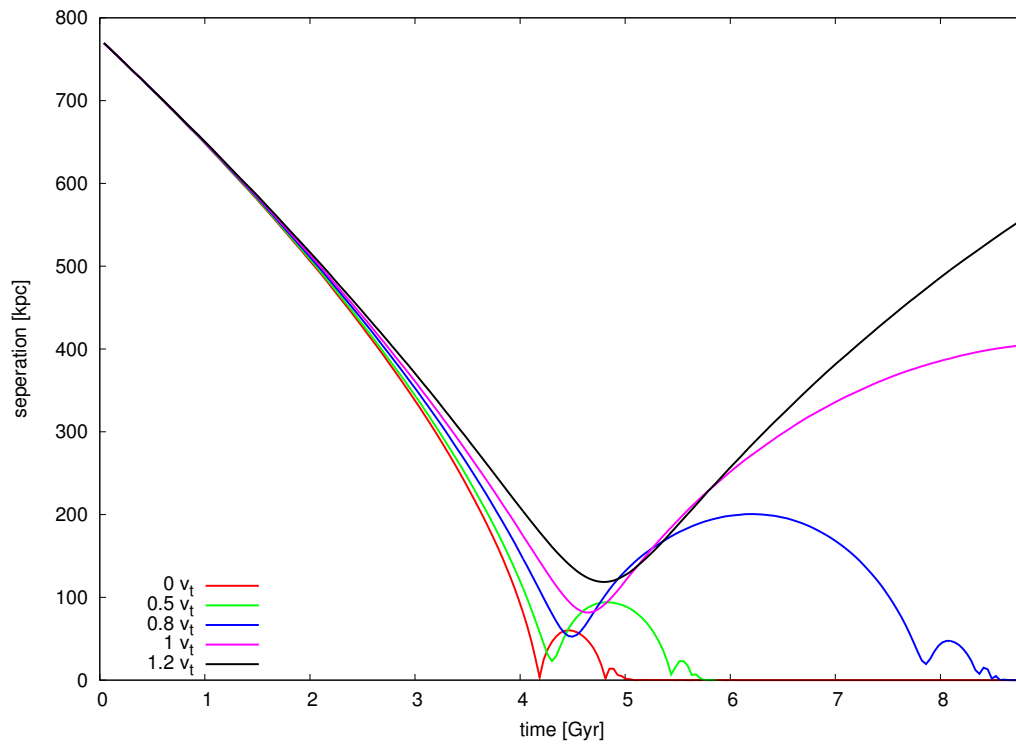


Figure 4.11: This plot shows the separation of M31 and the Milky Way evolving over time for different transverse velocities. The velocities are represented as fractions of 42 km/s. This data is taken from models Mv1, Mv0.5, Mv0.8 and Mv1.2. $N = 700,000$.

Total mass

To examine the effect of the the total mass of the Milky Way Andromeda system, we evaluated it with three different total masses, which range from, $\mathbf{M}_{\text{tot}} = 1.03 \cdot 10^{12} M_{\odot}$ to $\mathbf{M}_{\text{tot}} = 1.87 \cdot 10^{12} M_{\odot}$. In figures 4.12 and 4.13 the separation versus time is plotted for the two models we evaluated for this parameter study.

Outer edge of the halo

To examine the effect of the the size of Andromeda's halo system, we evaluated the Milky Way Andromeda system with three different radii for the outer edge. These radii range from, $\mathbf{R}_{\text{h,M31}} 99$ kpc to $\mathbf{R}_{\text{h,M31}} 350$ kpc. In figures 4.14 and 4.14 the separation versus time is plotted for the two models we evaluated for this parameter study. They show us that the influence from the change of the halo is noticeable at the end of our simulation.

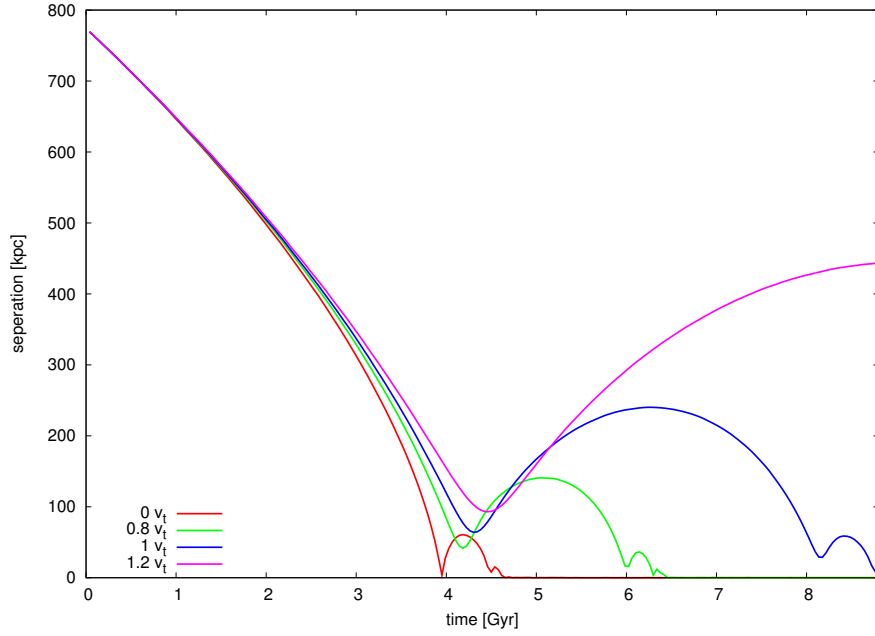


Figure 4.12: This plot shows the separation of M31 and the Milky Way evolving over time for different transverse velocities in a system where the total mass is increased with 30 %. The velocities are represented as fractions of 42 km/s. This data is taken from models Mm1.3v1, Mm1.3v0.5, Mm1.3v0.8 and Mm1.3v1.2. $N = 700,000$.

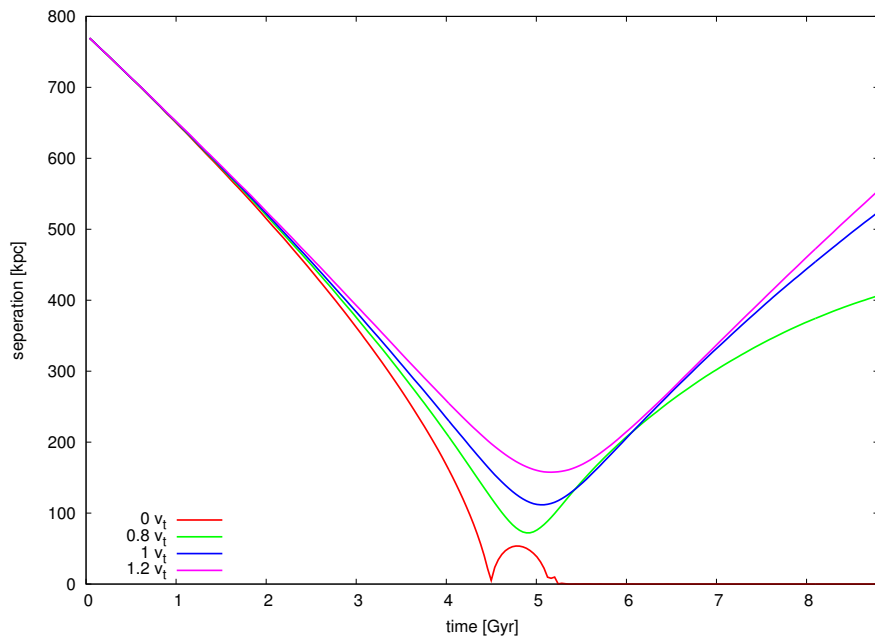


Figure 4.13: This plot shows the separation of M31 and the Milky Way evolving over time for different transverse velocities in a system where the total mass is decreased with 30 %. The velocities are represented as fractions of 42 km/s. This data is taken from models Mm0.7v1, Mm0.7v0.5, Mm0.7v0.8 and Mm0.7v1.2. $N = 700,000$.

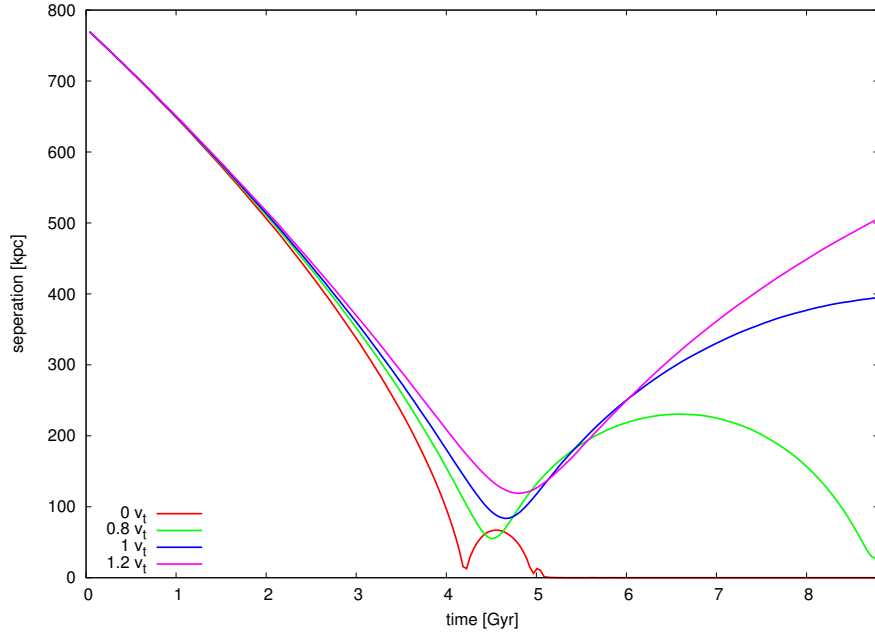


Figure 4.14: This plot shows the separation of M31 and the Milky Way evolving over time for different transverse velocities in a system where the halo edge of M31 is increased to 350 kpc. The velocities are represented as fractions of 42 km/s. This data is taken from models Mr350v1, Mr350v0.5, Mr350v0.8 and Mr350v1.2. $N = 700,000$.

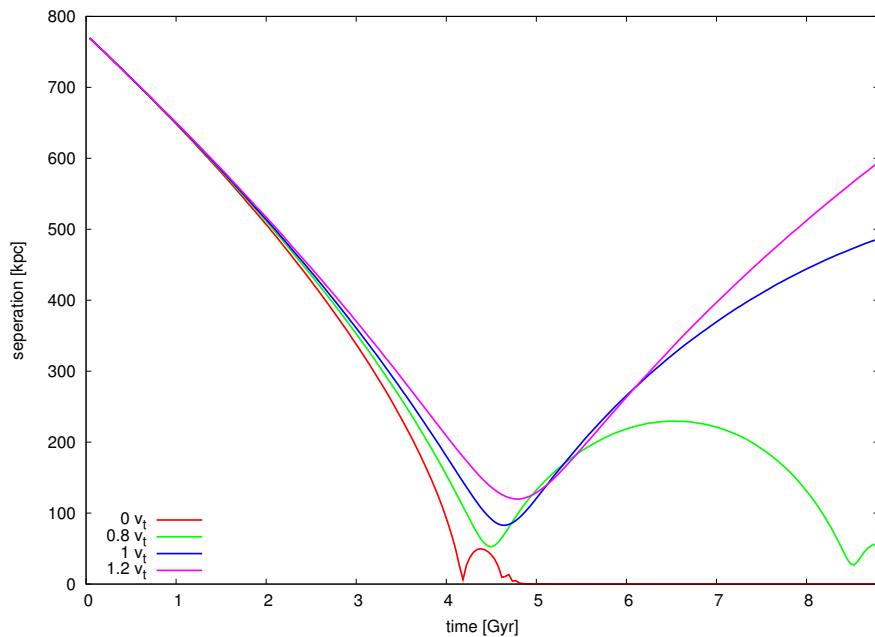


Figure 4.15: This plot shows the separation of M31 and the Milky Way evolving over time for different transverse velocities in a system where the halo edge of M31 is decreased to 100 kpc. The velocities are represented as fractions of 42 km/s. This data is taken from models Mr100v1, Mr100v0.5, Mr100v0.8 and Mr100v1.2. $N = 700,000$.

4.3 Formation of tidal tails

All of our models show formation of tidal tails. In model Mv0.5 the tidal tails are most present. Both systems have tidal tails, see figure 4.16, 4.17 and 4.18. We notice that Andromeda's tidal tails are much larger than the Milky Way's. This is the result of cumulative effect of having a more massive disk in a less massive halo in case of Andromeda. Figure 4.19 shows the change in Lagrangian radii and separation for the disk and bulge of the Milky Way and Andromeda Galaxy. Moments before first approach, the outer parts of the disk are compressed. This compression is followed by an expansion of the galactic core. At moment of second approach a similar effect takes place. For comparison we made similar plots, see figure of our model with increased transverse velocity, Mv0.8, B.1 and B.2.

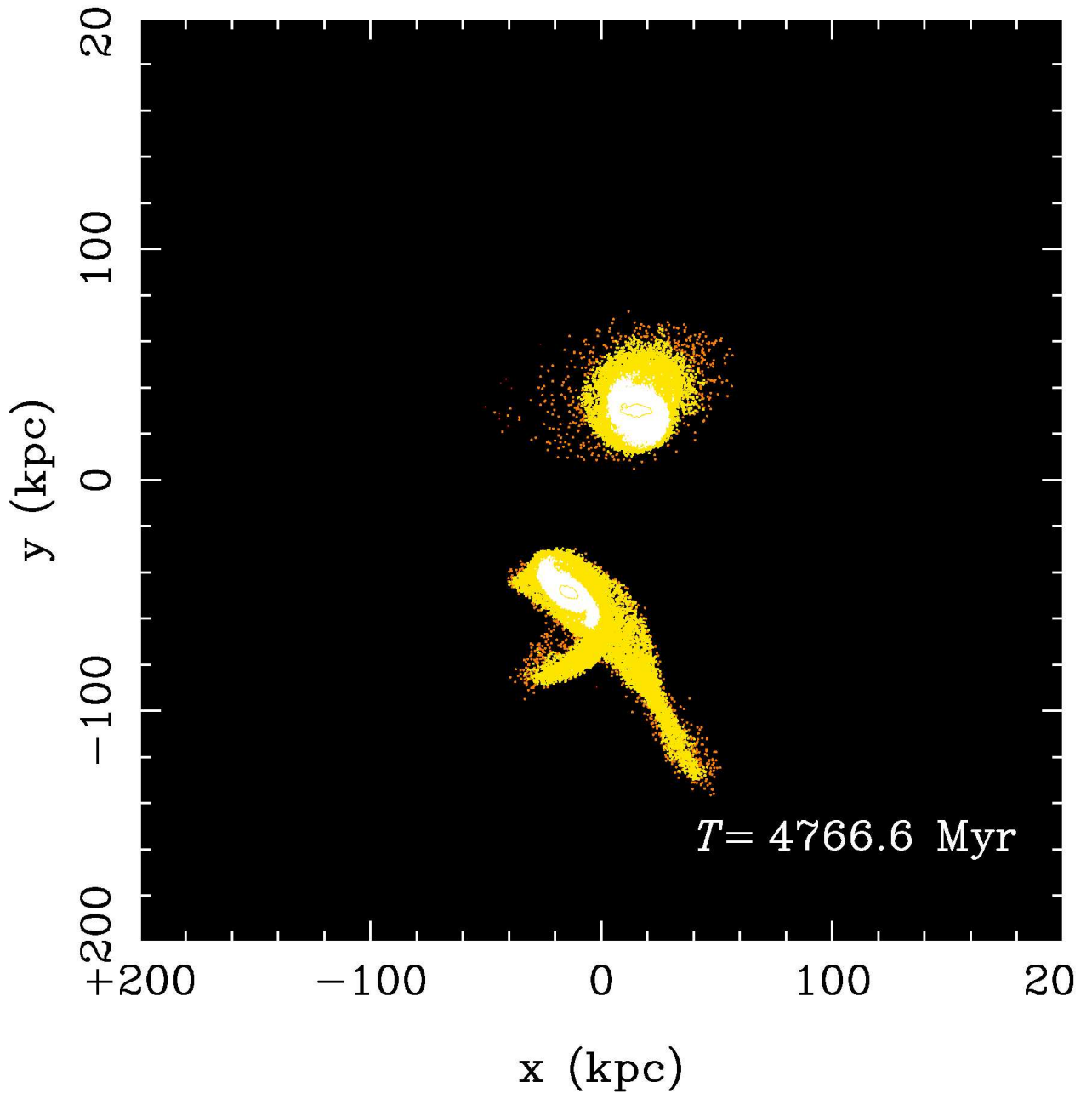


Figure 4.16: This figure shows the Milky Way (top) and the Andromeda galaxy (bottom) 400 million years after t_1 . Both galaxies show non-axisymmetric tidal features. Andromeda's tidal tails are longer. The yellow dots represent density. The increasing size and intensifying color corresponds with an increase of density. $N = 700,000$.

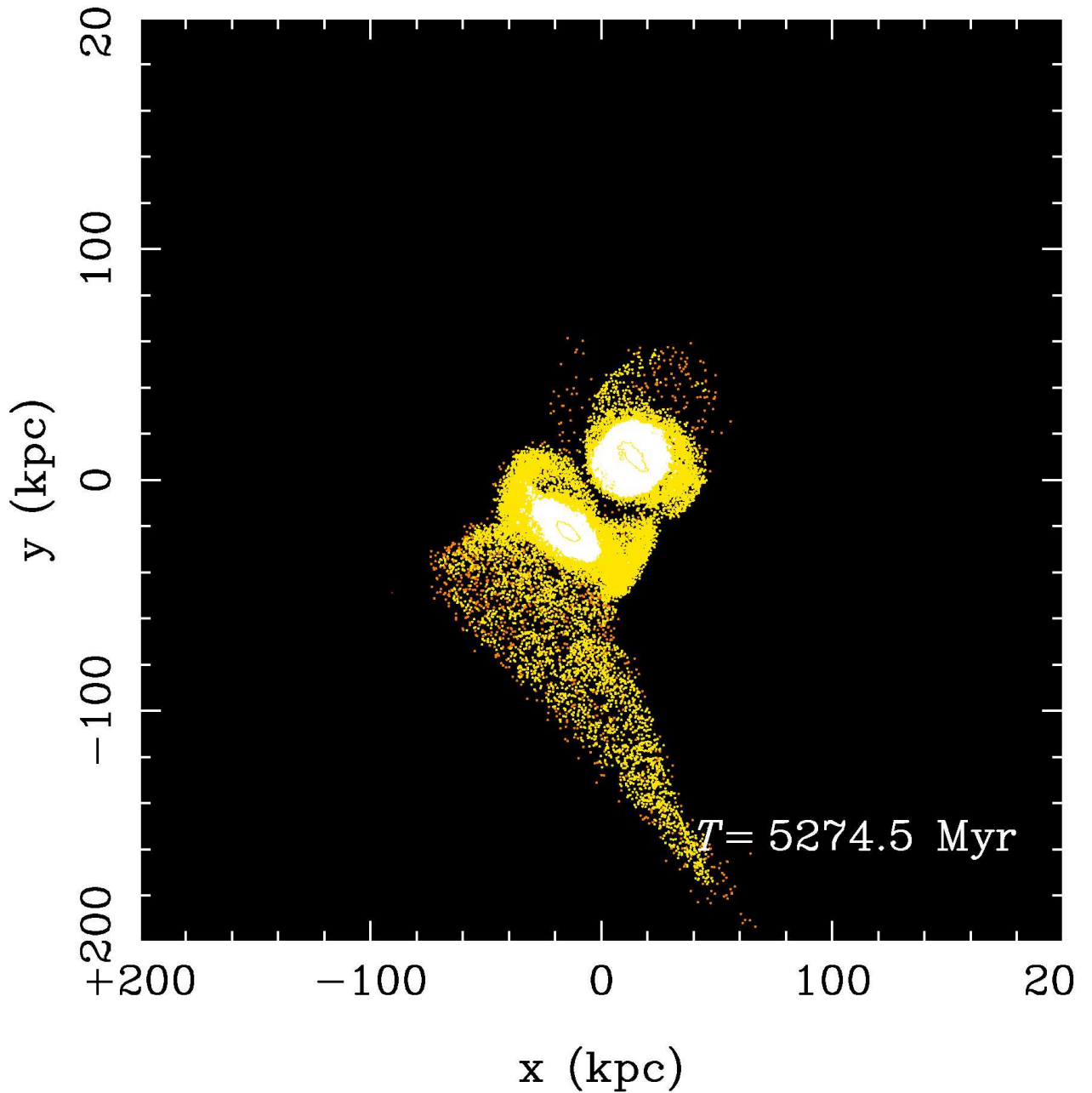


Figure 4.17: This figure shows the Milky Way (top) and the Andromeda galaxy (bottom) 200 million years before t_2 . Both galaxies start to merge. Andromeda's most predominant tidal tail is huge in comparison its one size. The yellow dots represent density. The increasing size and intensifying color corresponds with an increase of density. $N = 700,000$.

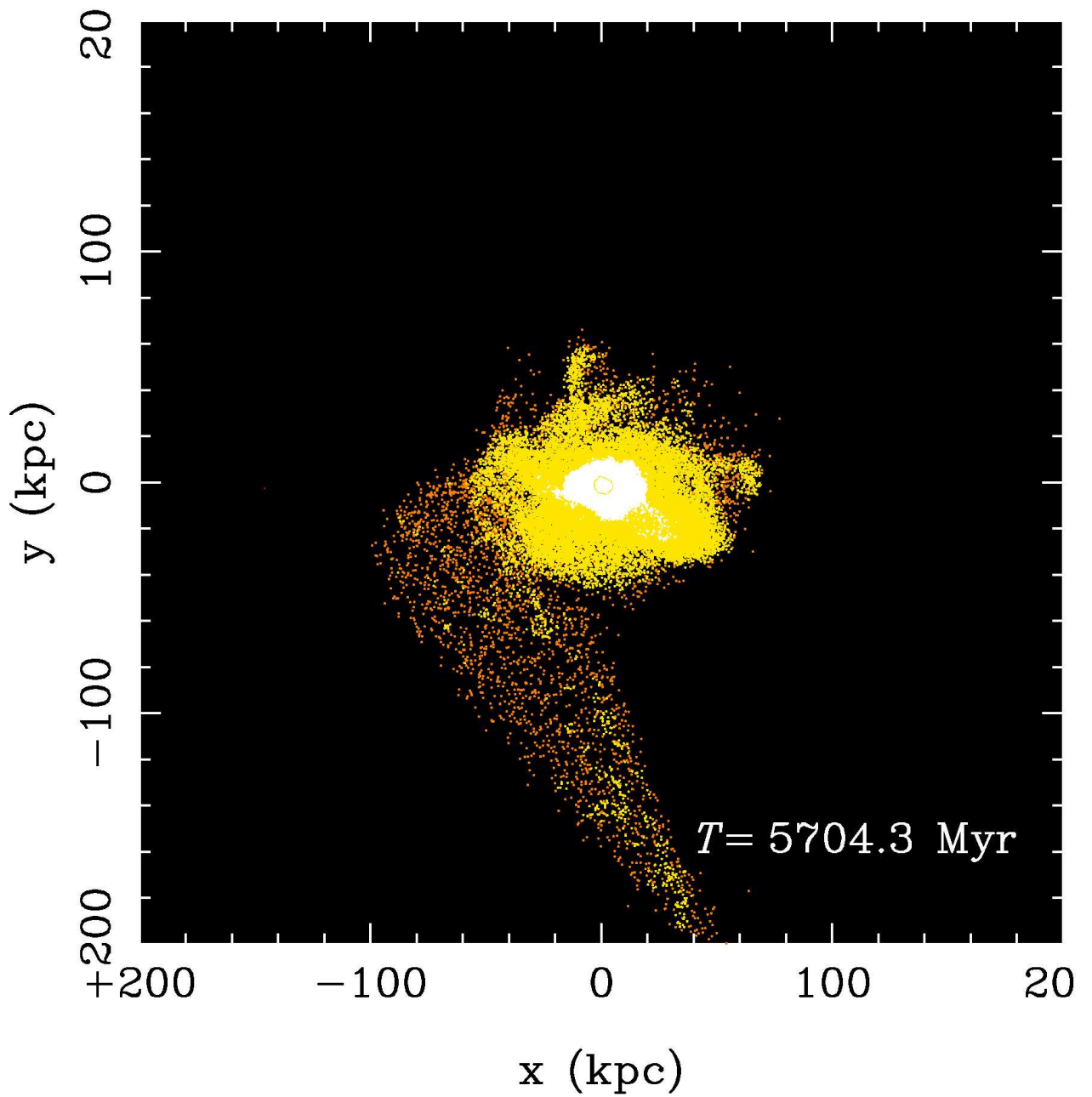


Figure 4.18: This figure shows the merger of the Milky Way and Andromeda. Andromeda's huge tidal tail is dissipating. The yellow dots represent density. The increasing size and intensifying color corresponds with an increase of density. $N = 700,000$.

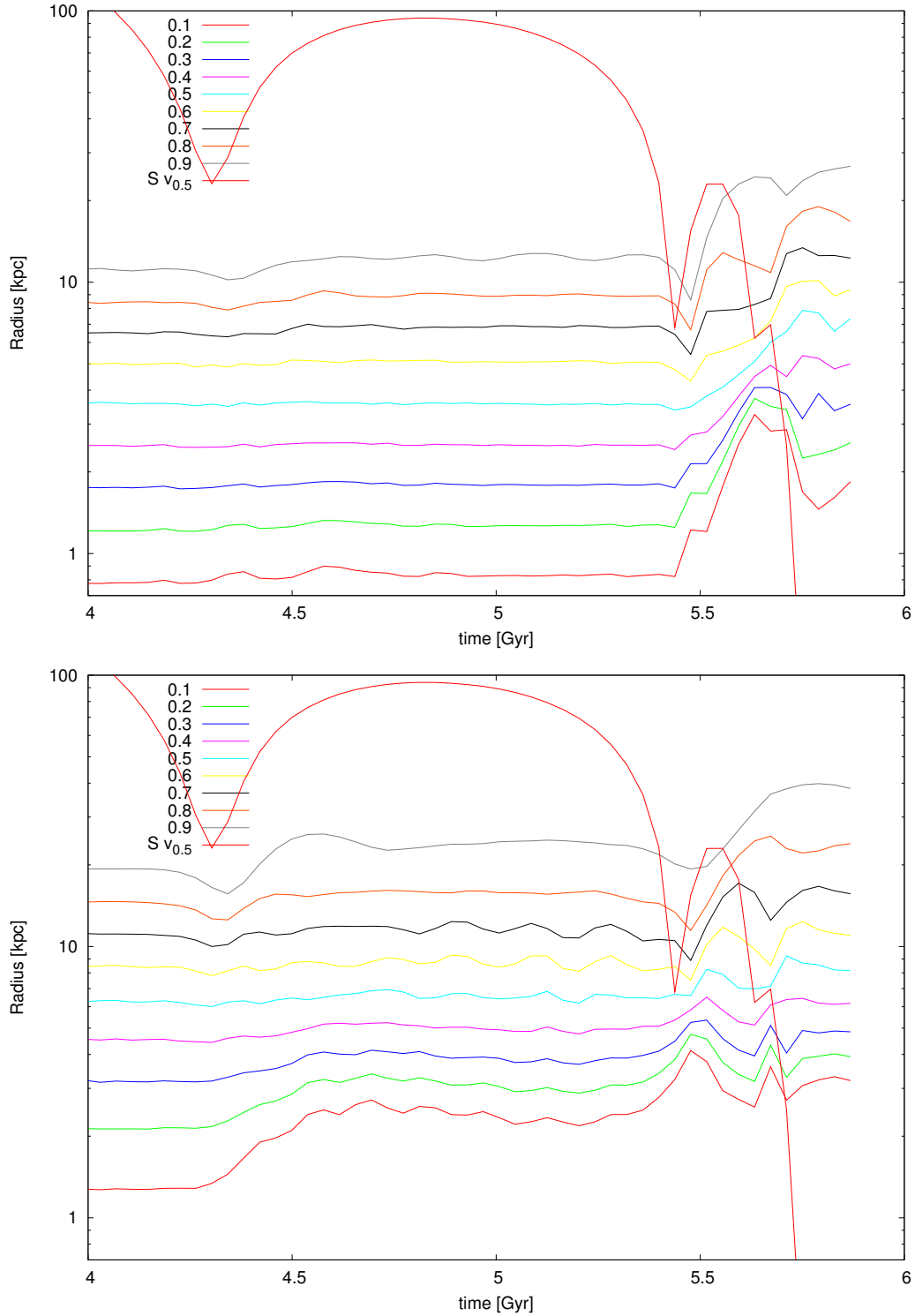


Figure 4.19: These plots show the radii of the Milky Way Galaxy (top) and the Andromeda Galaxy in terms of different mass fractions of the disk and bulge during a merger event. The initial transverse velocity in this model is 21 km/s. Also plotted is the separation. The radii of Andromeda change more then the radii of the Milky Way. This data is taken from model ‘Mv0.5’.

CHAPTER 5

Discussion

5.1 Mass produced by Galactics

There are various ways to find estimates for the mass of the Milky Way and Andromeda. In table 5.1 estimates of both masses are presented. The initial conditions of the models we use, found by Widrow and Dubinski (2005) produce low masses in comparison with the other values in literature. Evans and Wilkinson (2000) claim just like Widrow and Dubinski (2005) that the Milky Way is more massive than Andromeda. This is in contradiction with current opinion. Andromeda's rotation curve is ten percent higher than the Milky Way's. Also Andromeda contains the double amount of globular clusters, compared with the Milky Way. The Milky Way on the other hand has more infrared luminosity than Andromeda (Walterbos and Kennicutt, 1987) and its mass of hydrogen gas exceeds Andromeda's (Hodge, 1992). Evans and Wilkinson (2000) found an estimate by observing the line of sight velocities of objects that orbit Andromeda and the Milky Way and found masses which were \sim two times greater than the masses we chosen for our initial conditions. These objects are satellite galaxies, globular clusters and stellar halo planetary nebulae. Loeb *et al.* (2005) did something very similar, but only used the line of sight velocity of one of Andromeda's satellites, M33. These masses are the highest in current literature. Also Brunthaler *et al.* (2007) used the observed proper motion of two satellites to find the mass of Andromeda. Assuming the satellites are bound, they find a mass similar to ours. All these results could be enhanced by a larger number of tracers objects.

Cox and Loeb (2008) on the other hand, have constructed a N-body/hydronomical simulation. The masses they have chosen are also \sim two times higher than the masses we have chosen and are based on models created by Hernquist (1993) and favored by Klypin *et al.* (2002). These models use dark matter densities and other constraints, predicted by the standard cold dark matter (Λ CDM) cosmology.

In the models we used, the masses depend greatly on the input parameters of the fully self consistent disk bulge halo model, build by Kuijken and Dubinski (1995) and have many possible solutions. Widrow and Dubinski (2005) have found two particular models that fit observa-

| Article | Mass MW ($\times 10^{11} M_{\odot}$) | Mass M31 ($\times 10^{11} M_{\odot}$) |
|---------------------------------|---|--|
| Gott and Thuan (1978) | 11.5 | 11.5 |
| Kuijken and Dubinski (1995) | 3.17-19.5 | - |
| Dubinski <i>et al.</i> (1996) | 5-17 | 11-36 |
| Evans and Wilkinson (2000) | 19^{+36}_{-17} | 12.3^{+18}_{-6} |
| Widrow <i>et al.</i> (2003) | - | 4.15-12.7 |
| Widrow and Dubinski (2005)* | 7.8 | 6.8 |
| Loeb <i>et al.</i> (2005) | 23 | 34 |
| Brunthaler <i>et al.</i> (2007) | - | 7.5 |
| Heinsman (2008) | 19.5 | 19.5 |
| Cox and Loeb (2008) | 10 | 16 |
| test model | 8 | 12.8 |

Table 5.1: The mass of the Milky Way and Andromeda according to literature and a test model (see text). We used the masses estimated by Widrow and Dubinski (2005, indicated by *) in our models.

tional data and therefor provide realistic models.

It should be clear by now, that there are such a large variety of masses, mainly because the extent and density profile of the dark matter halo are still unknown. When we increase the cut-off parameter of the halos of both systems in our models we get values for the mass, which are more consistent in the literature, see table 5.1, test model. However these models do not fit the observational data. Therefor we favor the approach of Widrow and Dubinski (2005) and use there initial conditions in our models.

5.2 Mergers

In figure 5.1 the moments of first approach, second approach and merger are plotted for different transverse velocities. They are similar to the results found by Heinsman (2008), but slower. This is caused by the difference in total mass of the system. Only in two cases both systems merge. In both cases is the transverse velocity much smaller than the estimated value of 42 km/s.

In figure 5.2 we take different total masses in account and see that they influence the system much. For these plots we used data from the thesis from Heinsman (2008), for the values of moment of first approach, second approach and merger for $M_{\text{tot}} = 3.9 \cdot 10^{12} M_{\odot}$. Although our initial conditions are different, we believe we can use this data set for comparison. Figure 5.2 shows us the moments of first approach, second approach and merger. We varied mass over the range of masses suggested in the literature.

At \mathbf{v}_0 all models merge within the evaluated time. Notice also that we plotted the free fall estimate from equation (2.9) in the top left plot. This is the time it would take two point masses to collide under their own gravitational pull. They fit almost exactly. The difference between our results and the free fall time can be explained by the fact both galaxies experience dynamical friction, when their components overlap each other.

At $\mathbf{v}_{0.8}$ all models merge except for the least massive one. Moments of second approach lay very close to each other, but increase rapidly when the transverse velocity is increased.

At \mathbf{v}_1 only the most massive model merges, within the evaluated time. Extrapolating the fact that in the plots \mathbf{v}_0 and $\mathbf{v}_{0.8}$ the time of merger happens very quickly after the time second approach, we can assume that the moment of merger for $M_{\text{tot}} = 1.87 \cdot 10^{12} M_{\odot}$ happens just after 9 Gyr. We also assume that the time of second approach grows rapidly for increasing $\mathbf{v}_{\text{trans}}$ and decreasing mass, similar like the plot of $\mathbf{v}_{0.8}$.

At $\mathbf{v}_{1.2}$ none of our models, except the most massive one, even experience second approach and merger within the evaluated time.

When we compare our results with the results of Cox and Loeb (2008), we notice that they reach point of merger much faster. We predict that the moment of first approach and merger will be in 3 and 5 Gyr, taking no transverse velocity in account. They predict that these times are 2 and 5 Gyr. Their relative timescale for first approach is much quicker, although the time between first approach and merger is quicker in our models. We can account this difference to the more massive system they have used. But if we check the top left plot in figure 5.2 and see what time of first approach we would predict for $16 \cdot 10^{11} M_{\odot}$ we get a time of ~ 3.5 Gyr. The explanations for these discrepancies can be found in the fact that Cox and Loeb (2008) have assumed that their systems are embedded in a diffuse medium of dark matter and gas. The model we used lacks such a background potential. Dynamical friction seems to shorten the time of first approach. Cox and Loeb (2008) performed their simulations without the background potential and got much longer timescales. The moment of first approach

and merger are then 10 and 30 Gyr. This effect can be explained by equation (2.22). When we increase the background potential, we increase the density. In equation (2.22) the factor $(M + m)$ would increase. This results in an increase of $d\mathbf{v}/dt$. The models we used do not take in account a background potential. This should be looked into in the future.

Cox and Loeb (2008) took only the radial velocity component in account. Cosmological simulations predict that the transverse velocity component of Andromeda can be present, but should be much lower then the value found by van der Marel and Guhathakurta (2008). The reason for this discrepancy is still unclear. In figure 5.3 we have plotted the separation at

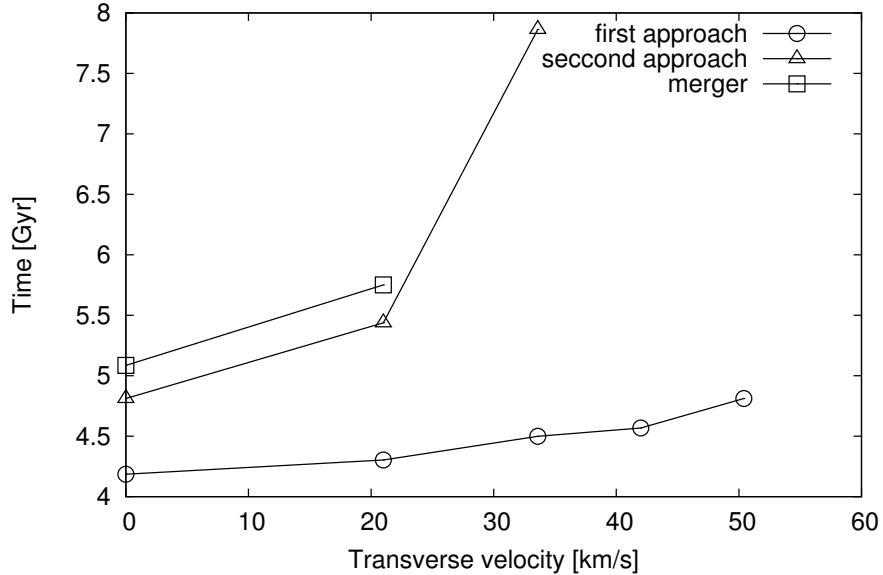


Figure 5.1: This plot shows the moments of first approach, second approach and merger for different transverse velocities. The velocities are represented as fractions of 42 km/s. This data is taken from models Mv1, Mv0.5, Mv0.8 and Mv1.2. $N = 700,000$.

moment of first approach for different total mass and transverse velocities. We also put in two lines as reference. They are the combined halo and disk radii. We plotted the outer edges of the radii. Those outer edges have very low density, so when systems slightly overlap the resulted effect should be marginal. Notice that in three models the disks overlap at moment of first approach and that all models predict that the halos overlap at every moment of first approach. This plot shows also that at $\mathbf{v}_{\text{turns}} = 0$ the radial velocity component, \mathbf{v}_{rad} is not perfectly aligned to the line between Andromeda and the Milky Way. The two centers of density miss each other by a factor of three kpc. The outer edge of the bulge of the Milky way and Andromeda are 3 and 8 kpc for comparison.

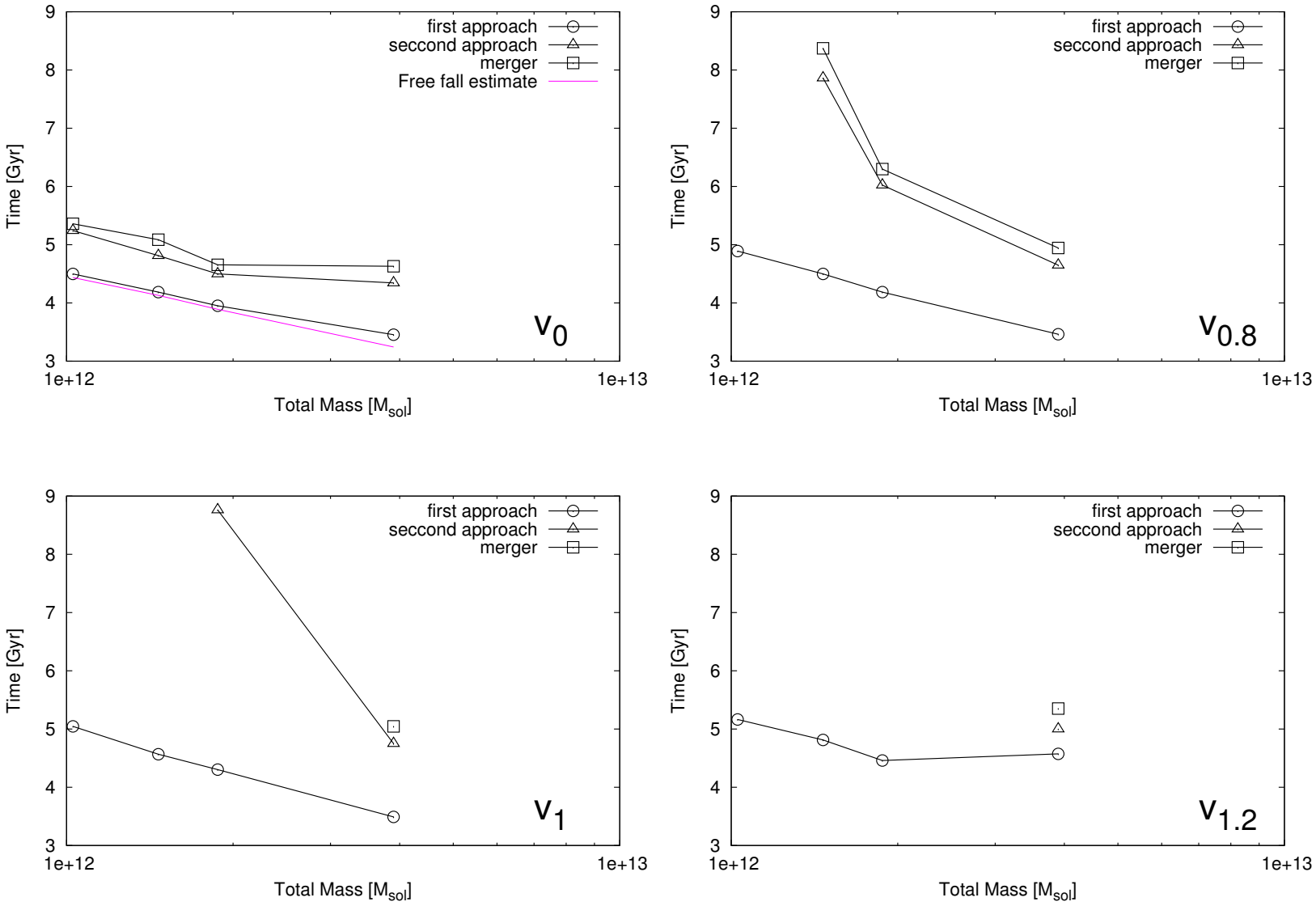


Figure 5.2: These four figures show the moments of first approach, second approach and merger for different transverse velocities and total mass of the system. These figures are made with data from our models Mv0 to Mm0.7v1.2 from table 4.1 and from the thesis by Heinsman (2008). v_0 , $v_{0.8}$, v_1 and $v_{1.2}$ correspond with 0, 33.6, 42 and 50.4 km/s.

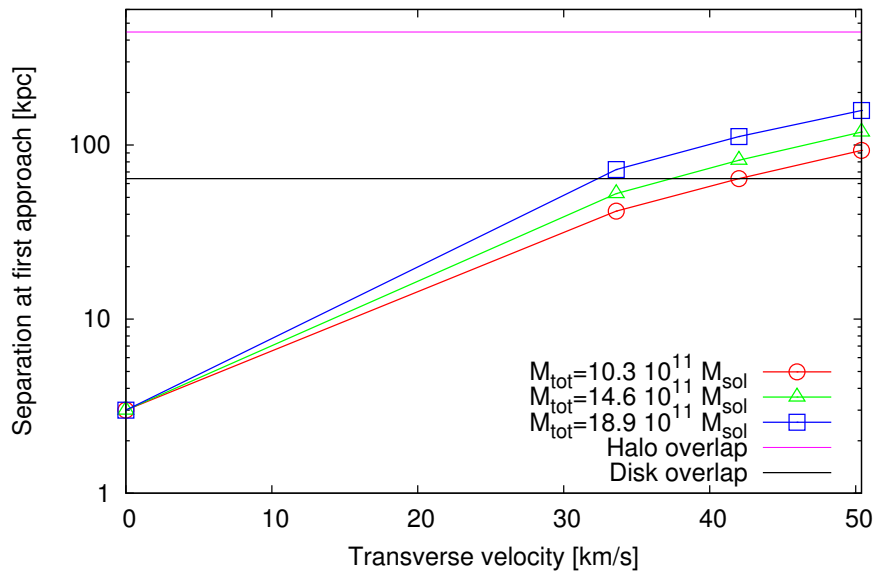


Figure 5.3: This figure shows the separation between the Milky Way and Andromeda at moment of first approach different transverse velocities and different total mass. We have also plotted the combined radii of both disks and halo, to see if the systems overlap.

5.3 Size of Andromeda's halo

We also looked into the effect of an elongated halo of Andromeda, while keeping the total mass the same. We expected to detect effects caused by the change in dynamical friction. In the figure 5.4 the results are plotted. Here is the time of first approach plotted versus change of halo. We detected no significant effect. We realize that moment of first approach is the least effected by changing the Andromeda halo and that effects can be seen in moments of second approach and merger. The evaluation time we used, 9 Gyr, is too short to witness significant effects. Although one can see in figure 4.14 and 4.15 at the end of the evaluation differences caused by change in dynamical friction.

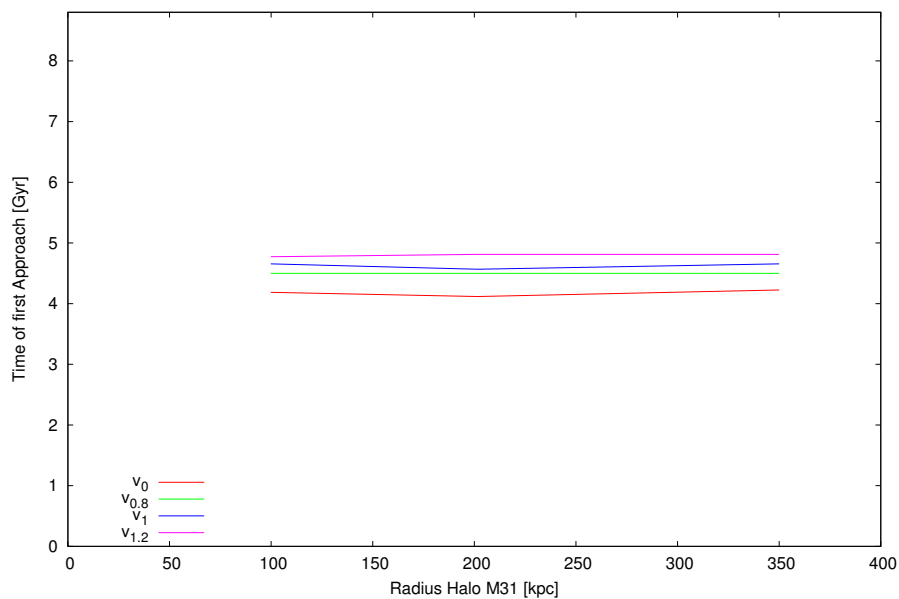


Figure 5.4: This figure shows the moment of first approach for different halo sizes for Andromeda.

5.4 Expanding bulge

We did not expect the contraction of the disk and expansion of the bulge, when they undergo a merger, as seen in figure 4.19. The apparent decrease of density in the bulge can influence the dynamics of super massive black holes in galaxy mergers. We recommend a simulation with higher particle numbers and smaller time steps to find out if this effect really takes place.

5.5 Conclusion

From figure 5.3 we can conclude that, when assuming Andromeda has $v_{\text{trans}} = 42$ km/s, models exceeding total mass of $M_{\text{tot}} = 18.7 \cdot 10^{11} M_{\odot}$ will merge in the next 9 Gyr, according to our models. The total mass resulting from our initial conditions is smaller than $M_{\text{tot}} = 18.7 \cdot 10^{11} M_{\odot}$. This means that according to our models Andromeda and the Milky Way will not merge in the next 9 Gyr, but will experience the moment of first approach in 4.5 Gyr. Taking into account that for decreasing total mass the time of second approach grows rapidly, we also conclude that according to our initial conditions it will take at least two times the current age of the universe when Andromeda will start merging with the Milky Way. This is considerably longer, compared with current opinion. In the end the mass and dynamics of the Local Group can only be understood, when we know the mass and dynamics of the Milky Way and Andromeda Galaxy.

Acknowledgments

First I want to thank dr. S. Portegies Zwart and dr. S. Harfst, for giving me the opportunity to do this project and for supervising me during it. Simon's enthusiasm and Stefan's realism are together a perfect couple for difficult students like me. I would like to point out that I really enjoyed the given independence and freedom during this project.

I especially want to thank drs. E. Heinsman for her support during this thesis. She helped me approach some aspects of my research from different angles. I know this sounds very general, but it is true. You really supported me on this. I also want to thank my parents, who called me every single day (!) for the last months, asking how the work on my thesis went and if I shouldn't be at university.

Finally I like to thank SARA for providing me with computer time and their quick customer support.

APPENDIX A

Used derivations

Galactics units

The units in table 2.1 are chosen, so that $G = 1$. For the moment we will denote this changed constant as G_{gal} . It is common to take $G = 1$, when performing N-body simulations on computers Heggie and Mathieu (1986). We check our units first by taking the regular cgs G_{cgs} ,

$$G_{\text{cgs}} \equiv 6.67 \cdot 10^{-8} [\text{cm}^3 \text{g}^{-1} \text{s}^{-2}] \quad (\text{A.1})$$

and change it to 1 by dividing it with itself,

$$G_{\text{gal}} \equiv 1 = \frac{G_{\text{cgs}}}{6.67 \cdot 10^{-8}}. \quad (\text{A.2})$$

Now we plug in the units given by Galactics and perform a unit analyze.

$$G_{\text{gal}} = \frac{\hat{r}^3}{\hat{m}\hat{t}^2} \frac{1}{6.67 \cdot 10^{-8}} \quad (\text{A.3})$$

$$G_{\text{gal}} = \frac{(1 \cdot 10^3 \text{pc})^3}{2.33 \cdot 10^9 M_{\odot} 9.781 \cdot 10^6 \text{yr}} \frac{1}{6.67 \cdot 10^{-8}} \quad (\text{A.4})$$

Now we enter

$$\text{pc} = 3.085677582 \cdot 10^{18} \text{cm} \quad (\text{A.5})$$

$$M_{\odot} = 1.989 \cdot 10^{33} \text{g} \quad (\text{A.6})$$

$$\text{yr} = 3.1558149984 \cdot 10^7 \text{s} \quad (\text{A.7})$$

in equation (A.4). This gives

$$G_{\text{gal}} = 1 \quad (\text{A.8})$$

QED

Rotation

Andromeda’s spin axes is not parallel to the the Milky Way’s. So before we translate M31 to the proper coordinates, we have to rotate it. We can rotate an arbitrary vector, using equation

$$\mathbf{r}_{M31} = \mathbf{R}_{M31}\mathbf{r}. \quad (\text{A.9})$$

In equation (A.9) \mathbf{r}_{M31} is defined as the rotated \mathbf{r} and \mathbf{R}_{M31} is defined as the rotation matrix. In order to find this matrix we have to do some steps. I use the recipe given by Murray (1983), McConnachie and Irwin (2006) and Metz *et al.* (2007).

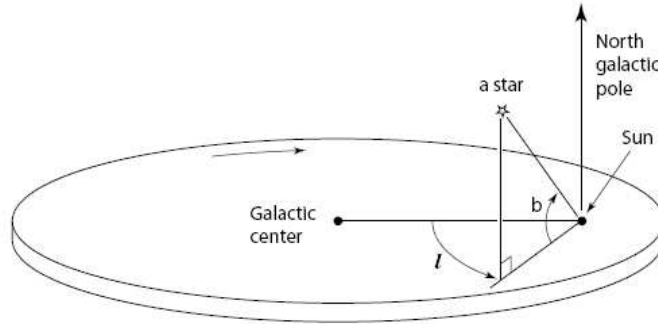


Figure A.1: Galactic coordinates (l, b) as explained and taken from the book by (Binney and Tremaine, 1987, chap. 1.1).

There are many different coordinates systems in astrometrics. We could use Galactic or celestial coordinate systems. The most common coordinate system in astronomy is the celestial J2000 system or equatorial coordinate system, using right ascension and declination (α, δ) in the Julian 2000 epoch, see figure A.2. Another coordinate system used in extragalactic astronomy is the Galactic coordinate system (l, b) , as described in Binney and Tremaine (1987, chap. 1.1), see figure A.1. Although using Galactic coordinates seems more logical in our thesis, it is not a clever choice, because almost all literature uses the J2000 system. Also the orientation of M31 is conventionally given in equatorial coordinates in the literature by de Vaucouleurs (1958). Using the equatorial coordinate system also eliminates the time dependent differences between the celestial plane and the Galactic plane, because we did not use Galactic coordinates.

First let the Cartesian unity vector $(\mathbf{e}_x^{M31}, \mathbf{e}_y^{M31}, \mathbf{e}_z^{M31})$ be centered in M31 similar to $(\mathbf{e}_x^{MW}, \mathbf{e}_y^{MW}, \mathbf{e}_z^{MW})$. We define \mathbf{e}_z^{M31} such that it is parallel with Andromeda’s spin axis and \mathbf{e}_x^{M31} such that it is parallel with Andromeda’s disk in the direction of the Milky Way and $\mathbf{e}_y^{M31} = \mathbf{e}_z^{M31} \times \mathbf{e}_x^{M31}$.

Now we calculate the “normal triad” as described in the book *Vectorial Astrometry* by Murray (1983).

$$\mathbf{R}_{rpq}(\alpha, \delta) = (\mathbf{e}_r, \mathbf{e}_p, \mathbf{e}_q) \quad (\text{A.10})$$

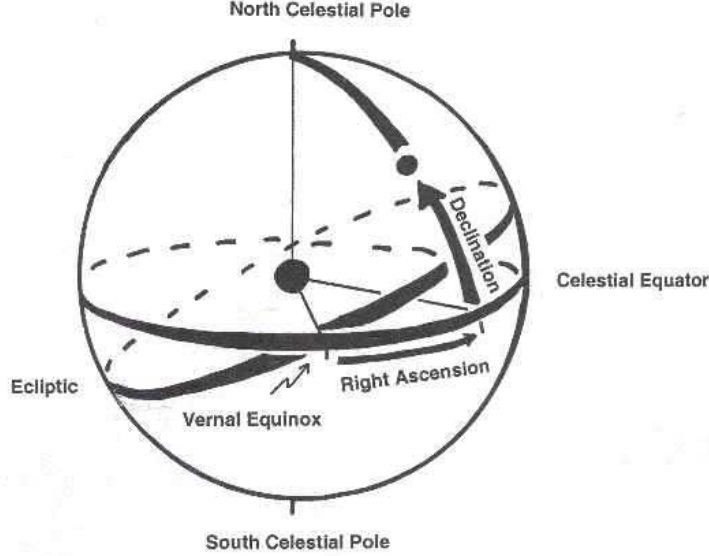


Figure A.2: Right ascension and Declination in the equatorial coordinate system.

$$= \begin{pmatrix} \cos \delta \cos \alpha & -\sin \alpha & -\sin \delta \alpha \\ \cos \delta \sin \alpha & \cos \alpha & -\sin \delta \sin \alpha \\ \sin \delta & 0 & \cos \delta \end{pmatrix} \quad (\text{A.11})$$

The matrix $\mathbf{R}_{\mathbf{rpq}}$ rotates $(\mathbf{e}_x^{\text{MW}}, \mathbf{e}_y^{\text{MW}}, \mathbf{e}_z^{\text{MW}})$ to $(\mathbf{e}_r, \mathbf{e}_p, \mathbf{e}_q)$. In equation (A.11) the α and the δ are the right ascension and declination of M31. Now is \mathbf{e}_r pointing the same direction as (α, δ) of M31, \mathbf{e}_p towards the north celestial pole and \mathbf{e}_q towards the east, parallel with the celestial equator, see figure A.3.

The next step is incorporating the i , inclination, and the θ , position angle, given by de Vaucouleurs (1958). This can be done by equation (A.12).

$$\mathbf{R}'_{\text{M31}} = \mathbf{R}_y(90^\circ - i)\mathbf{R}_x(90^\circ - \theta)\mathbf{R}_{\mathbf{rpq}}(\alpha, \delta) \quad (\text{A.12})$$

Both \mathbf{R}_x and \mathbf{R}_y are the standard unit axis rotational matrices. To rotate a vector for ξ degrees over the x -axis we can use

$$\mathbf{R}_x \equiv \begin{pmatrix} 1 & 0 & 0 \\ 0 & \cos \xi & -\sin \xi \\ 0 & \sin \xi & \cos \xi \end{pmatrix} \quad (\text{A.13})$$

and to rotate a vector for ζ degrees we can use

$$\mathbf{R}_y \equiv \begin{pmatrix} \cos \zeta & 0 & -\sin \zeta \\ 0 & 1 & 0 \\ \sin \zeta & 0 & \cos \zeta \end{pmatrix}. \quad (\text{A.14})$$

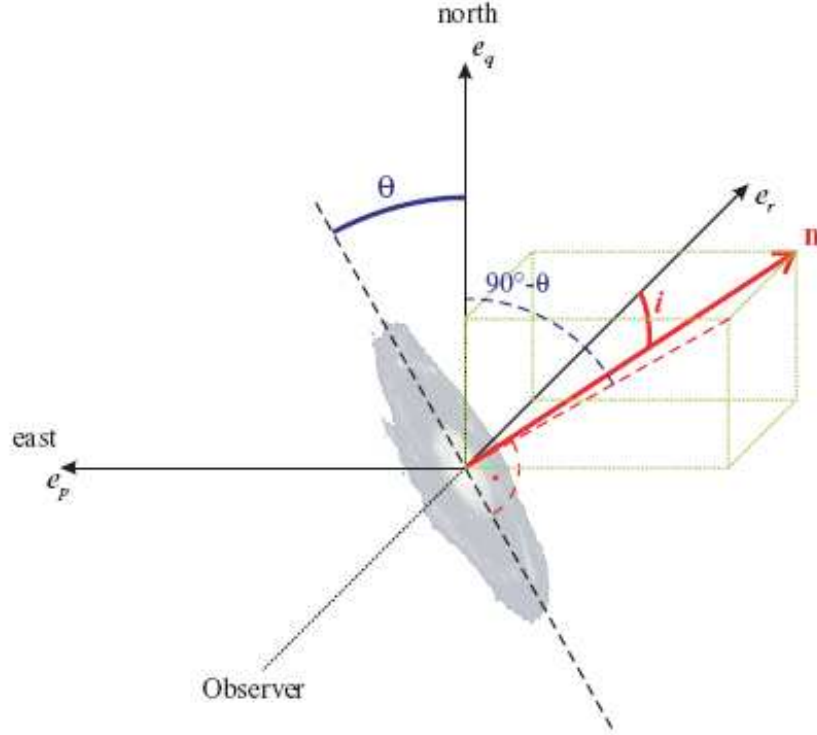


Figure A.3: Andromeda's normal \mathbf{n} , with the “normal triad” $(\mathbf{e}_r, \mathbf{e}_p, \mathbf{e}_q)$. Also is shown the inclination θ and position angle i . (Photo credit: Metz *et al.* (2007))

Now we can calculate \mathbf{R}'_{M31} using equation (A.12). This is basically the matrix we need, to properly rotate our M31 model in the right orientation. We adopt the apostrophe, because there are still some steps we need to do before this matrix is correct. We used the J2000 system to give a value for the orientation of M31. J2000 is a heliocentric system, but in the end we need the orientation of M31 in a Galactic centric perspective. So we need to add one other rotation matrix in equation (A.12) of the order of

$$\arctan(8.5\text{kpc} / 770\text{kpc}) = 0^\circ 6. \quad (\text{A.15})$$

Where 8.5 kpc is the distance from the sun to the Galactic center (GC) and 770 kpc is the distance between the sun and M31.

To find a rotation matrix to compensate for this we first need to find the vector pointing from Andromeda to the Galactic Center to the Sun,

$$\mathbf{r}'(\text{GC}) = \mathbf{R}'_{M31}(\mathbf{r}(\text{M31}) - \mathbf{r}(\text{GC})). \quad (\text{A.16})$$

Then we have to project this vector on the plane of M31,

$$\mathbf{r}'_{xy}(\text{GC}) = \mathbf{e}_x^{M31}(\mathbf{e}_x^{M31} \cdot \mathbf{r}'(\text{GC})) + \mathbf{e}_y^{M31}(\mathbf{e}_y^{M31} \cdot \mathbf{r}'(\text{GC})). \quad (\text{A.17})$$

Now can we calculate the angle between this vector and the vector $\mathbf{e}_x^{\text{M31}}$:

$$\eta = \arccos \left(\frac{\mathbf{r}'_{xy}(\text{GC}) \cdot \mathbf{e}_x^{\text{M31}}}{|\mathbf{r}'_{xy}(\text{GC})|} \right). \quad (\text{A.18})$$

This angle we can use in the standard z -rotation matrix. Similar to matrix (A.13) and (A.14), we can define

$$\mathbf{R}_z \equiv \begin{pmatrix} \cos \eta & \sin \eta & 0 \\ -\sin \eta & \cos \eta & 0 \\ 0 & 0 & 1 \end{pmatrix}. \quad (\text{A.19})$$

So the total rotation matrix \mathbf{R}_{M31} then becomes

$$\mathbf{R}_{\text{M31}} = \mathbf{R}_z(\eta) \mathbf{R}_y(90^\circ - i) \mathbf{R}_x(90^\circ - \theta) \mathbf{R}_{\text{rpq}}(\alpha, \delta) \quad (\text{A.20})$$

$$= \begin{pmatrix} 0.7703 & 0.3244 & 0.5490 \\ -0.6321 & 0.5017 & 0.5905 \\ -0.0839 & -0.8019 & 0.5915 \end{pmatrix} \quad (\text{A.21})$$

Now we can multiply the rotation matrix, R , with the position vector, (x, y, z) , and the velocity vector (V_x, V_y, V_z) in the Galactics output data file.

APPENDIX B

Tables and Figures

| Parameter | Milky Way | Andromeda | Total system |
|--|------------|------------|--------------|
| Galactics Model | MWb | M31a | Mv1 |
| Number of particles, N | 350,000 | 350,000 | 700,000 |
| Total Mass [$2.33 \cdot 10^9 M_\odot$] | 335.232666 | 293.737518 | 628.97018 |
| Disk Mass [$2.33 \cdot 10^9 M_\odot$] | 15.1457396 | 34.1285782 | - |
| Bulge Mass [$2.33 \cdot 10^9 M_\odot$] | 5.10096455 | 12.3888931 | - |
| Halo Mass [$2.33 \cdot 10^9 M_\odot$] | 314.985962 | 247.220047 | - |
| Disk Edge [kpc] | 32 | 32 | - |
| Bulge Edge [kpc] | 3.05999994 | 8.05999947 | - |
| Halo Edge, R_{IC} [kpc] | 244.48999 | 201.619995 | - |
| M_{MW}/M_{M31} | - | - | 1.1412661 |
| Halo Edge $-R_{IC}$ | 0 | 0 | - |

Table B.1: In this table the mass and radii are show for the two models we created using Galactics for the initial conditions. In this table we define the edge of the halo as R_{IC} . It is used in table B.2, B.3, B.4 and B.5 for comparison.

| Parameter | Milky Way | Andromeda | Total system |
|--|------------|------------|--------------|
| Galactics Model | MW-Mm1.3 | M31-M1.3 | Mm1.3 |
| Number of particles, N | 350,000 | 350,000 | 700,000 |
| Total Mass [$2.33 \cdot 10^9 M_\odot$] | 434.915588 | 381.313568 | 806.229 |
| Disk Mass [$2.33 \cdot 10^9 M_\odot$] | 15.3201466 | 34.3820877 | - |
| Bulge Mass [$2.33 \cdot 10^9 M_\odot$] | 4.88541937 | 11.9496078 | - |
| Halo Mass [$2.33 \cdot 10^9 M_\odot$] | 414.710022 | 334.981873 | - |
| Disk Edge [kpc] | 32 | 32 | - |
| Bulge Edge [kpc] | 2.8599999 | 7.57999992 | - |
| Halo Edge [kpc] | 244.279999 | 201.25 | - |
| M_{MW}/M_{M31} | - | - | 1.1405720 |
| Halo Edge $- R_{IC}$ [kpc] | 0.21000 | 0.369995 | |

Table B.2: In this table the properties are show for the two models we created using Galactics with 30 % more mass.

| Parameter | Milky Way | Andromeda | Total system |
|--|------------|------------|--------------|
| Galactics Model | MW-Mm0.7 | M31-Mm0.7 | Mm0.7 |
| Number of particles, N | 350,000 | 350,000 | 700,000 |
| Total Mass [$2.33 \cdot 10^9 M_\odot$] | 234.721725 | 205.965042 | 440.687 |
| Disk Mass [$2.33 \cdot 10^9 M_\odot$] | 15.0134411 | 33.7906303 | - |
| Bulge Mass [$2.33 \cdot 10^9 M_\odot$] | 5.19716072 | 12.6609087 | - |
| Halo Mass [$2.33 \cdot 10^9 M_\odot$] | 214.511124 | 159.513504 | - |
| Disk Edge [kpc] | 32 | 32 | - |
| Bulge Edge [kpc] | 3.18999982 | 8.48999977 | - |
| Halo Edge [kpc] | 244.369995 | 201.87999 | - |
| M_{MW}/M_{M31} | - | - | 1.1396192 |
| Halo Edge $- R_{IC}$ | 0.119995 | 0.259995 | |

Table B.3: In this table the properties are show for the two models we created using Galactics with 30 % less mass.

| Parameter | Milky Way | Andromeda | Total system |
|--|------------|------------|--------------|
| Galactics Model | MW-Mr1.3 | M31-Mr1.3 | Mr1.3 |
| Number of particles, N | 350,000 | 350,000 | 700,000 |
| Total Mass [$2.33 \cdot 10^9 M_\odot$] | 335.232666 | 293.712372 | 628.97018 |
| Disk Mass [$2.33 \cdot 10^9 M_\odot$] | 15.1457396 | 33.4306374 | - |
| Bulge Mass [$2.33 \cdot 10^9 M_\odot$] | 5.10096455 | 12.6104088 | - |
| Halo Mass [$2.33 \cdot 10^9 M_\odot$] | 314.985962 | 247.671326 | - |
| Disk Edge [kpc] | 32 | 32 | - |
| Bulge Edge [kpc] | 3.05999994 | 8.92000008 | - |
| Halo Edge, | 244.48999 | 350 | - |
| $M_{\text{MW}}/M_{\text{M31}}$ | - | - | 1.1413638 |

Table B.4: In this table the properties are show for the two models we created using Galactics for system with a enlarged halo edge for Andromeda. It is now 350 kpc instead of 200 kpc. Notice that the mass is similar to the values in table B.1.

| Parameter | Milky Way | Andromeda | Total system |
|--|------------|------------|--------------|
| Galactics Model | MW-Mr0.7 | M31-Mr0.7 | Mr0.7 |
| Number of particles, N | 350,000 | 350,000 | 700,000 |
| Total Mass [$2.33 \cdot 10^9 M_\odot$] | 335.232666 | 293.276428 | 628.97018 |
| Disk Mass [$2.33 \cdot 10^9 M_\odot$] | 15.1457396 | 34.5876694 | - |
| Bulge Mass [$2.33 \cdot 10^9 M_\odot$] | 5.10096455 | 10.7247066 | - |
| Halo Mass [$2.33 \cdot 10^9 M_\odot$] | 314.985962 | 247.96405 | - |
| Disk Edge [kpc] | 32 | 32 | - |
| Bulge Edge [kpc] | 3.05999994 | 6.63999987 | - |
| Halo Edge, | 244.48999 | 99.8399963 | - |
| $M_{\text{MW}}/M_{\text{M31}}$ | - | - | 1.1430604 |

Table B.5: In this table the properties are show for the two models we created using Galactics for system with a shortened halo edge for Andromeda. It is now 100 kpc instead of 200 kpc. Notice that the mass is similar to the values in table B.1.

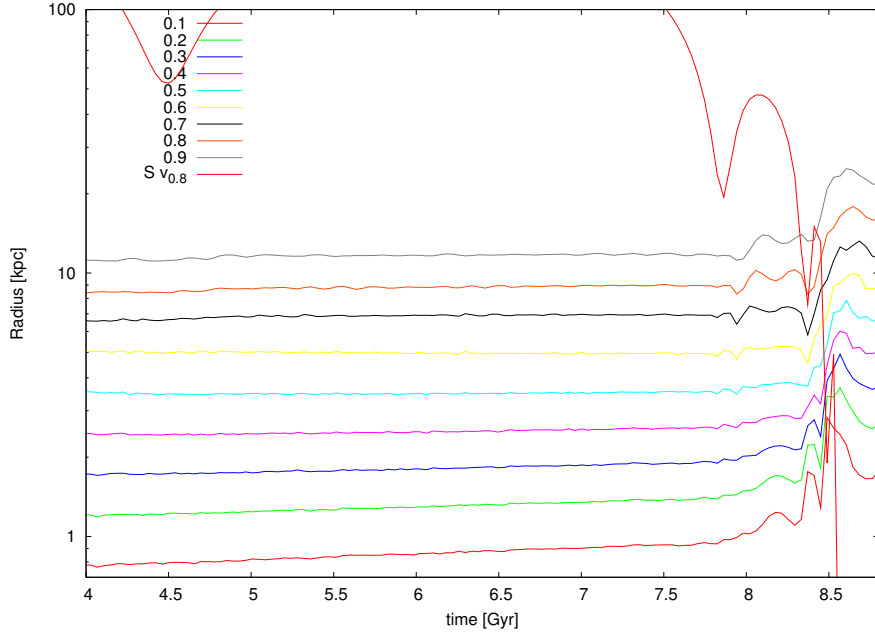


Figure B.1: This plot shows radii of the Milky Way Galaxy in terms of different mass fractions of the disk and bulge during a merger event. This data is taken from model ‘Mv0.8’.

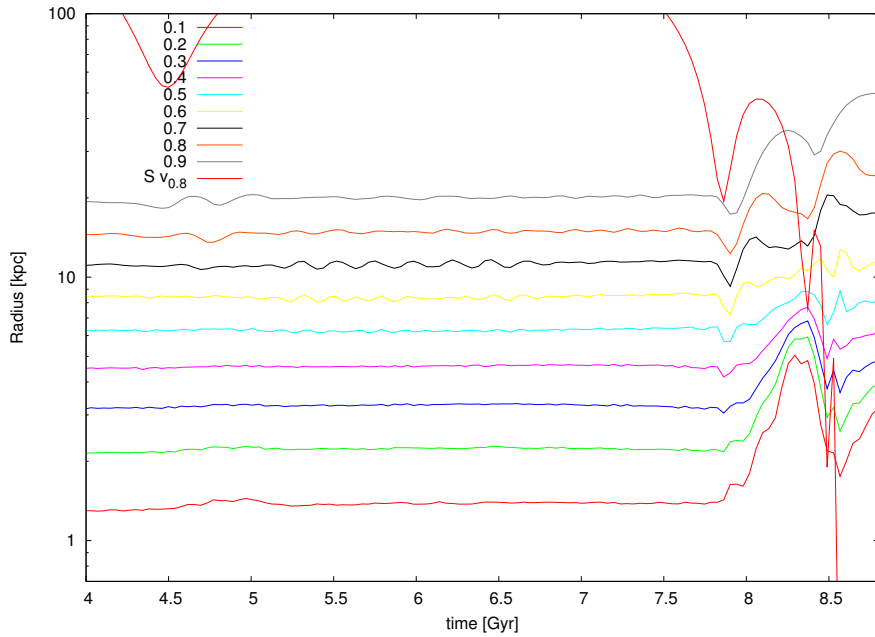


Figure B.2: This plot shows radii of the Milky Way Galaxy in terms of different mass fractions of the disk and bulge during a merger event. This data is taken from model ‘Mv0.8’.

APPENDIX C

Nederlandse samenvatting

Andromeda is net als de Melkweg een spiraal sterrenstelsel, en samen met enkele andere satelliet stelsels vormen we de Lokale Groep. Andromeda staat ongeveer 700.000 keer verder weg, van de Aarde, dan de dichtstbijzijnde ster. Veel dynamische eigenschappen van de beide stelsels zijn nog steeds in grote mate onbekend. Zo zijn de massa's van beide stelsel nog onbekend. De orde van grote van de massa wordt geschat op 10^{12} zonnemassa's. De rede dat we zo weinig weten van de massa's is dat beide stelsels voor een groot deel uit donkere materie bestaan. We weten niet hoe de dichtheid van dit materiaal verloopt ten opzichte van radius. Waarschijnlijk bevindt de donkere materie van beide stelsels zich in een bol om het zichtbare deel van de sterrenstelsels. Deze bollen kunnen zeer groot zijn en elkaar zelf overlappen.

Een eigenschap die wel goed bekend is, is de snelheid waarmee Andromeda naar ons toe vliegt, de zogenaamde radiale snelheid. Deze snelheid bedraagt 117 km/s. Deze waarde is makkelijk de meten met behulp van Doppler verschuiving van het licht, wat uitgezonden wordt door Andromeda. Aan de andere kant is de transversale snelheid, die precies loodrecht op de radiale snelheid staat nog onbekend. Al wordt deze in een recent artikel geschat op een waarde van 42 km/s.

Vanwege deze onzekerheden is de baan van Andromeda ten opzichte van de Melkweg nog grotendeels onbekend. In deze scriptie hebben we de meest recente geschatte waarden van deze baanparameters verzameld. Vervolgens hebben we deze parameters gebruikt om een model te maken van het Melkweg Andromeda systeem. Deze parameters hebben we ook gevarieerd over een bereik dat een groot deel van de literatuur beslaat. Zo hebben we de transversale snelheid gevarieerd tussen 0 en ongeveer 50 km/s. De totale massa van het systeem hebben gevarieerd tussen $1 \cdot 10^{12}$ tot $4 \cdot 10^{12}$ zonnemassa's. We hebben ook nog gekeken naar de effecten van de grootte van de donkere materie bol om het Andromeda stelsel.

We hebben al deze modellen geëvalueerd met behulp van computers. Het bijzondere aan deze computers is dat we de zwaarste delen van de berekeningen hebben uitgevoerd op de meest recente videokaart van NVIDIA. Deze kaarten hebben de potentie om supercomputers

te vervangen, vanwege relatief lage kosten en hoge snelheid.

Wij kunnen concluderen dat, gebruikmakend van onze beginwaarden, het onwaarschijnlijk is dat de Melkweg binnen twee huidige leeftijden het heelal botst met Andromeda, al wordt dit niet aangenomen in huidige opinie binnen de literatuur.

APPENDIX D

Used abbreviations

b = Galactic Latitude
dec = Declination
yr = year
Gyr = 10^9 year
 l = Galactic longitude
ly = light year $\approx 9.5 \cdot 10^{17}$ cm
M31 = Andromeda galaxy
MW = Milky Way Galaxy
 M_{tot} = total mass
 M_{d} = disk mass
 M_{b} = bulge mass
 M_{h} = halo mass
 n = number density of particles
 N = number of particles
 n_* = number density of stars
pc = parsec $\approx 3 \cdot 10^{18}$ cm
kpc = kiloparsec $\approx 3 \cdot 10^{21}$ cm
RA = Right Ascension
 R_{gc} = Distance from galactic center
 v_r = radial velocity
yr = year
 v_{trans} = transverse velocity

Bibliography

- Aschenbach, B. (2005). Mass and Angular Momentum of Sgr A*. In A. Merloni, S. Nayakshin, and R. A. Sunyaev, editors, *Growing Black Holes: Accretion in a Cosmological Context*, pages 302–303.
- Barnes, J. and Hut, P. (1986). A Hierarchical O(NlogN) Force-Calculation Algorithm. *Nature*, **324**, 446–449.
- Beckwith, S. V. W., Stiavelli, M., Koekemoer, A. M., Caldwell, J. A. R., Ferguson, H. C., Hook, R., Lucas, R. A., Bergeron, L. E., Corbin, M., Jogee, S., Panagia, N., Robberto, M., Royle, P., Somerville, R. S., and Sosey, M. (2006). The Hubble Ultra Deep Field. *AJ*, **132**, 1729–1755.
- Binney, J. and Dehnen, W. (1997). The outer rotation curve of the Milky Way. *MNRAS*, **287**, L5–L7.
- Binney, J. and Tremaine, S. (1987). *Galactic Dynamics*. Princeton Series in Astrophysics. Princeton University Press, Princeton, U.S.A.
- Braun, R. (1991). The distribution and kinematics of neutral gas in M31. *ApJ*, **372**, 54–66.
- Brunthaler, A., Reid, M. J., Falcke, H., Henkel, C., and Menten, K. M. (2007). Proper Motions in the Andromeda Subgroup. *ArXiv e-prints*, **708**.
- Chandrasekhar, S. (1943). Dynamical Friction. I. General Considerations: the Coefficient of Dynamical Friction. *ApJ*, **97**, 255–+.
- Courteau, S. and van den Bergh, S. (1999). The Solar Motion Relative to the Local Group. *AJ*, **118**, 337–345.
- Cox, T. J. and Loeb, A. (2008). The collision between the Milky Way and Andromeda. *MNRAS*, **386**, 461–474.
- Curtis, H. D. (1917). Novae in the Spiral Nebulae and the Island Universe Theory. *PASP*, **29**, 206–207.
- de Vaucouleurs, G. (1958). Photoelectric photometry of the Andromeda nebula in the UBV system. *ApJ*, **128**, 465–+.

- Dubinski, J., Mihos, J. C., and Hernquist, L. (1996). Using Tidal Tails to Probe Dark Matter Halos. *ApJ*, **462**, 576–+.
- Easton, C. (1913). A Photographic Chart of the Milky way and the Spiral Theory of the Galactic System. *ApJ*, **37**, 105–+.
- Evans, N. W. and Wilkinson, M. I. (2000). The mass of the Andromeda galaxy. *MNRAS*, **316**, 929–942.
- Ewen, H. I. and Purcell, E. M. (1951). Observation of a Line in the Galactic Radio Spectrum: Radiation from Galactic Hydrogen at 1,420 Mc./sec. *Nature*, **168**, 356–+.
- Gott, III, J. R. and Thuan, T. X. (1978). Angular momentum in the local group. *ApJ*, **223**, 426–436.
- Heggie, D. C. and Mathieu, R. D. (1986). Standardised Units and Time Scales. In P. Hut and S. L. W. McMillan, editors, *The Use of Supercomputers in Stellar Dynamics*, volume 267 of *Lecture Notes in Physics*, Berlin Springer Verlag, pages 233–+.
- Heinsman, E. (2008). Goodbye Andromeda? Universiteit van Amsterdam - Astronomy and Astrophysics.
- Hernquist, L. (1993). N-body realizations of compound galaxies. *ApJS*, **86**, 389–400.
- Hodge, P. W., editor (1992). *The Andromeda galaxy*, volume 176 of *Astrophysics and Space Science Library*.
- Hubble, E. (1929a). A Relation between Distance and Radial Velocity among Extra-Galactic Nebulae. *Proceedings of the National Academy of Science*, **15**, 168–173.
- Hubble, E. P. (1927). The classification of spiral nebulae. *The Observatory*, **50**, 276–281.
- Hubble, E. P. (1929b). A spiral nebula as a stellar system, Messier 31. *ApJ*, **69**, 103–158.
- Kahn, F. D. and Woltjer, L. (1959). Intergalactic Matter and the Galaxy. *ApJ*, **130**, 705–+.
- Kent, S. M., Huchra, J. P., and Stauffer, J. (1989). The shape of the mass distribution in M31 from its globular cluster system. *AJ*, **98**, 2080–2085.
- Kepler, J., Brahe, T., and Rudolf II (1609). *Astronomia nova*. Heidelberg : G. Voegelinus.
- Kerr, F. J. and Lynden-Bell, D. (1986). Review of galactic constants. *MNRAS*, **221**, 1023–1038.
- Klypin, A., Zhao, H., and Somerville, R. S. (2002). Λ CDM-based Models for the Milky Way and M31. I. Dynamical Models. *ApJ*, **573**, 597–613.
- Kroeker, T. L. and Carlberg, R. G. (1991). The accuracy of galaxy masses from the timing argument. *ApJ*, **376**, 1–7.

- Kuijken, K. and Dubinski, J. (1995). Nearly Self-Consistent Disc / Bulge / Halo Models for Galaxies. *MNRAS*, **277**, 1341–+.
- Lauer, T. R., Faber, S. M., Groth, E. J., Shaya, E. J., Campbell, B., Code, A., Currie, D. G., Baum, W. A., Ewald, S. P., Hester, J. J., Holtzman, J. A., Kristian, J., Light, R. M., Ligynds, C. R., O’Neil, Jr., E. J., and Westphal, J. A. (1993). Planetary camera observations of the double nucleus of M31. *AJ*, **106**, 1436–1447.
- Levine, E. S., Blitz, L., and Heiles, C. (2006). The Spiral Structure of the Outer Milky Way in Hydrogen. *Science*, **312**, 1773–1777.
- Levine, E. S., Heiles, C., and Blitz, L. (2008). The Milky Way Rotation Curve and Its Vertical Derivatives: Inside the Solar Circle. *ApJ*, **679**, 1288–1298.
- Lin, C. C. and Shu, F. H. (1964). On the Spiral Structure of Disk Galaxies. *ApJ*, **140**, 646–+.
- Loeb, A., Reid, M. J., Brunthaler, A., and Falcke, H. (2005). Constraints on the Proper Motion of the Andromeda Galaxy Based on the Survival of Its Satellite M33. *ApJ*, **633**, 894–898.
- McConnachie, A. W. and Irwin, M. J. (2006). The satellite distribution of M31. *MNRAS*, **365**, 902–914.
- Metz, M., Kroupa, P., and Jerjen, H. (2007). The spatial distribution of the Milky Way and Andromeda satellite galaxies. *MNRAS*, **374**, 1125–1145.
- Muller, C. A. and Oort, J. H. (1951). Observation of a Line in the Galactic Radio Spectrum: The Interstellar Hydrogen Line at 1,420 Mc./sec., and an Estimate of Galactic Rotation. *Nature*, **168**, 357–358.
- Murray, C. A. (1983). *Vectorial astrometry*. Bristol: Adam Hilger, 1983.
- Navarro, J. F., Frenk, C. S., and White, S. D. M. (1996). The Structure of Cold Dark Matter Halos. *ApJ*, **462**, 563–+.
- Newton, I. (1686). *Philosophiae Naturalis Principia Mathematica*. London Reg. Soc. Praeses.
- Nyland, L., Harris, M., and Prins, J. (2004). Poster presented at The ACM Workshop on General Purpose Computing on Graphics Hardware. Los Angeles, CA.
- Oort, J. H. (1941). Note on the structure of the inner parts of the galactic system. *BAIN*, **9**, 193–+.
- Oort, J.-H. (1953). L’Hydrogène interstellaire. *Ciel et Terre*, **69**, 117–+.
- Portegies Zwart, S. F., Belleman, R. G., and Geldof, P. M. (2007). High-performance direct gravitational N-body simulations on graphics processing units. *New Astronomy*, **12**, 641–650.

- Reber, G. (1944). Cosmic Static. *ApJ*, **100**, 279–+.
- Ribas, I. (2004). Distances and fundamental properties of eclipsing binaries in the LMC and M31. In R. W. Hilditch, H. Hensberge, and K. Pavlovski, editors, *Spectroscopically and Spatially Resolving the Components of the Close Binary Stars*, volume 318 of *Astronomical Society of the Pacific Conference Series*, pages 261–269.
- Seigar, M. S., Kennefick, D., Kennefick, J., and Lacy, C. H. S. (2008). Discovery of a Relationship between Spiral Arm Morphology and Supermassive Black Hole Mass in Disk Galaxies. *ApJ*, **678**, L93–L96.
- Slipher, V. M. (1913). The radial velocity of the Andromeda Nebula. *Lowell Observatory Bulletin*, **2**, 56–57.
- Smith, S. (1936). The Mass of the Virgo Cluster. *ApJ*, **83**, 23–+.
- Spergel, D. N., Bean, R., Doré, O., Nolta, M. R., Bennett, C. L., Dunkley, J., Hinshaw, G., Jarosik, N., Komatsu, E., Page, L., Peiris, H. V., Verde, L., Halpern, M., Hill, R. S., Kogut, A., Limon, M., Meyer, S. S., Odegard, N., Tucker, G. S., Weiland, J. L., Wollack, E., and Wright, E. L. (2007). Three-Year Wilkinson Microwave Anisotropy Probe (WMAP) Observations: Implications for Cosmology. *ApJS*, **170**, 377–408.
- Strom, K. M. and Strom, S. E. (1982). Galactic evolution - A survey of recent progress. *Science*, **216**, 571–580.
- Toomre, A. (1964). On the gravitational stability of a disk of stars. *ApJ*, **139**, 1217–1238.
- Toomre, A. (1981). What amplifies the spirals. In S. M. Fall and D. Lynden-Bell, editors, *Structure and Evolution of Normal Galaxies*, pages 111–136.
- van der Marel, R. P. and Guhathakurta, P. (2008). M31 Transverse Velocity and Local Group Mass from Satellite Kinematics. *ApJ*, **678**, 187–199.
- Walterbos, R. A. M. and Kennicutt, Jr., R. C. (1987). Multi-color photographic surface photometry of the Andromeda galaxy. *A&AS*, **69**, 311–332.
- Widrow, L. M. and Dubinski, J. (2005). Equilibrium Disk-Bulge-Halo Models for the Milky Way and Andromeda Galaxies. *ApJ*, **631**, 838–855.
- Widrow, L. M., Perrett, K. M., and Suyu, S. H. (2003). Disk-Bulge-Halo Models for the Andromeda Galaxy. *ApJ*, **588**, 311–325.
- Wong, T., Blitz, L., Kawamura, A., Iritani, H., and Fukui, Y. (2008). Atomic and Molecular Gas in Disk Galaxies. In K. Wada and F. Combes, editors, *Mapping the Galaxy and Nearby Galaxies*, pages 206–+.
- Wyse, R. F. G., Gilmore, G., and Franx, M. (1997). Galactic Bulges. *ARA&A*, **35**, 637–675.
- Zwicky, F. (1933). Die Rotverschiebung von extragalaktischen Nebeln. *Helvetica Physica Acta*, **6**, 110–127.